People's Democratic Republic of Algeria
Ministry of Higher Education and Scientific Research

University M'Hamed BOUGARA – Boumerdes

Institute of Electrical and Electronic Engineering

Department of Power and Control

Final Year Project Report Presented in Partial Fulfilment of the Requirements for the Degree of

MASTER

In **Power Engineering**

Option: **Power Engineering**

Title:

Design and implementation of Direct Torque Control of Induction Motor Drive

Presented by:

- **ROUIDJALI Imene**
- **REZKI Abdelaziz**

Supervisor:

Dr. METIDJI Brahim

Registration Number:……/2018

Dedications

I would like to dedicate this work to my lovely supportive family,

To my Grand-parents may their souls rest in peace,

To my parents, who have been a source of encouragement and inspiration to me throughout my life,

To my sisters Nassima and Dhaouia,

To my brother Amine,

To my Kung fu family,

To everyone whom whenever I felt down they helped me to stand up again and work harder .

Imene ROUIDJALI

I dedicate this work to my parents,

My brothers and sisters,

And to all my friends.

AZIZ

Acknowledgement

There have been many people who have walked alongside us during this year, this long busy year. They have guided us, placed opportunities in front of us and showed us the doors that might be useful to open. We would like to thank every one of them.Without hesitation we would especially like to thank our supervisor ***Dr.Brahim Metidji***, ***Dr.Abdelkarim Ammar*** and ***Mr Mehdi Sellali***. Without your encouragements, your belief in us, your help and inspiration this thesis would not have been possible.

Even though we found some difficulties during the realization of this thesis but our supervisor ***Dr B.Metidji*** as strict as he was but with good attention that we could understand only at the end gave us faith in ourself and in our skills, he showed us not to be scared and to try, to think and take risks as an engineer, to try to find solution to any obstacles we might face as we faced a lot.

So thank you again as we learnt a lot of technical skills during this amazing experience.

Abstract

The direct torque control was proposed as an alternative strategy to the field-oriented control for AC machines drive. This method consists on the direct determination of inverter switching states and offers a simpler and robust scheme and less sensitivity to machine parameters as it depends only on the stator resistance.

In this work, the direct torque is presented for induction motor drive fed by two-level voltage source inverter. The control algorithm has been investigated through simulation and experimental tests. The simulation part was carried out using MATLAB/Simulink software, the obtained results shows the effectiveness of this method. Moreover, the generic model of a direct torque control for induction machines is implemented using DSP TMS 320f28027f in order to test and validate the presented control algorithm.

Keywords: Induction motor, Direct torque control, Two-level inverter, Hysteresis controllers, DSP.

List of figures

List of tables

List of abbreviations

I.M	Induction Motor
E.M.F	Electro-motif Force
M.M.F	Magneto-motive Force
F.O.C	Field Oriented Control
D.T.C	Direct Torque Control
S.M.C	Sliding Mode Control
V.S.C	Variable Structure Control
V.S.I	Voltage Source Inverter
C.S.I	Current Source Inverter
P.I.D	Proportional Integral Derivative
T.H.D	Total Harmonic Distortion
F.F.T	Fast Fourier Transform
D.S.P	Digital signal Processing

Table of symbols

Variable	Description
VA, VB, VC	Instantaneous values of the stator phase voltages
*i*A, *i*B, *i*C	Instantaneous values of the stator phase currents
ΨA, ΨB, ΨC	Flux linkages of the stator phase windings
kA, kB, kC	Arbitrary phase variables
a, a^2	Spatial operators $a=e^{j2\pi/3}$ and $a^2=e^{j4\pi/3}$
α, β	Stator orthogonal coordinate system
D,Q	Direct and quadratic coordinate system
isα,β	Stator currents [A]
Vsα,β	Stator voltages [V]
Rs	Stator phase resistance [Ohm]
Rr	Rotor phase resistance [Ohm]
L s	Stator phase inductance [H]
L r	Rotor phase inductance [H]
L m	Mutual (stator to rotor) inductance [H]
ω /ωs	Electrical rotor speed/synchronous speed [rad/s]
P	Number of pole pairs
Te	Electromagnetic torque [Nm]

Table of contents

Chapter 01 : Background about induction motor

Chapter 2: Direct Torque Control for Induction Motor

Chapter 3: Simulation results of the D.T.C

Chapter 4: Simulation results of the D.T.C

General introduction

The rising fuel prices and pollution has lead to an increasing demand for electric vehicles in developed and emerging countries such as Germany, the US, China and Japan[02].

In electric vehicle, the control objective is the torque of the driving machine. Therefore, the innovation of the direct torque control [11] or the direct self-torque control [07] and [08] by Isao Takahashi and Toshihiko Noguchi has revolutionized the global market especially the one of induction motor as it was the first electrical machine where this technique has been applied and later on more developed techniques based on the DTC had been discovered.

This master work deals with one of the most famous and robust control methods for the induction motors which is the direct torque control. This report is divided into four chapters . The first one is an overview about the induction motors ,it includes its structure , principle of operation ,mathematical model and different available control strategies of the I.M. Then the second chapter is about the needed background about the D.T.C . After that , the third chapter consists of the simulation of all the mathematical models of the induction motor and the algorithm of the D.T.C using Matlab/Simulink v2018 .The results of this simulation is also mentioned in this chapter .Last but not least, the fourth chapter which consist of the implementation of the proposed D.T.C in order to validate the theory.Thus,a test bench composed of a 1.8kW squirrel-cage motor ,Semikron inverter,DSP TMS320f28027,Dspace interface card , current and voltage hall effect sensors' LA25-P and LV 25-V respectively circuits and 3 phase power supply .The DSP TMS320f28027f is programmed using C2000 Matlab package .

At the end a general conclusion and further work plans are proposed.

1.1. Introduction

Over the past years, DC machines were extensively used for variable speed applications. But due to their main inconvenient which is the presence of brush assembly and commentator, their drives became disused nowadays in the industry[01].

The low-cost, robustness, the higher performance and also the simple maintenance of the asynchronous motor make them advantageous in several industrial applications[04].

The squirrel cage induction motors known as the workhorses of the industry are the most widely used comparing with the other electrical motors worldwide and for different applications.

It has been noticed from the global electric market analysis, a great grow of induction machines and their drives especially in electric or hybrid vehicle market [15]. Recently the best and most known electrical vehicles like Tesla cars, Ix3 BMW all use induction motor.

All these factors make us interested more about the induction motor.

In this chapter, a review about the most relevant concepts about the induction motor is presented from its construction, principle of operation, its mathematical model to the different control strategies used in the industry in order to control it.

1.2. Construction and principal of operation of an induction motor

1.2.1. Construction of an induction motor

An induction motor is a type of asynchronous AC motor where power is supplied to the rotating device by means of electromagnetic induction. The general structure of an IM is depicted in figure 1.1 [01].

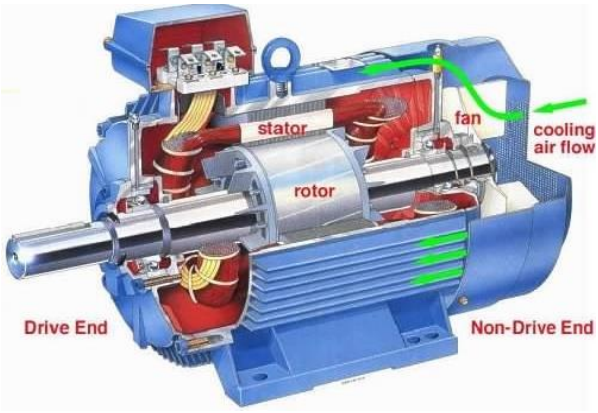

Fig. 1.1- Induction motor Structure

Like any other electrical motor , induction motor also have two main electromagnetic parts:

- Stationary part called the stator ;
- And a rotating part called the rotor, supported at each end on bearings.

Both the stator and the rotor are composed of:

- An electric circuit, usually made of insulated copper or aluminum to carry the current.
- A magnetic circuit, usually made from laminated steel, to carry magnetic flux.

a- Stator :

The stator is the fixed part of the motor. A cast iron or light alloy frame surrounds a ring of thin laminations (around 0.5 mm thick) made of silicon steel. The lamination of the magnetic circuit reduces losses via hysteresis and eddy currents. The laminations have slots in them for holding the stator windings that produce the rotating field (three windings for a 3-phase motor) .Each winding is made up of a number of coils. The way these coils are joined to one another defines the number of pair's poles of the motor, and thus the speed rotation.

The structure of the stator is illustrated in both figures 1.2 and 1.3[3].

Fig. 1.2-An overview of the stator structure

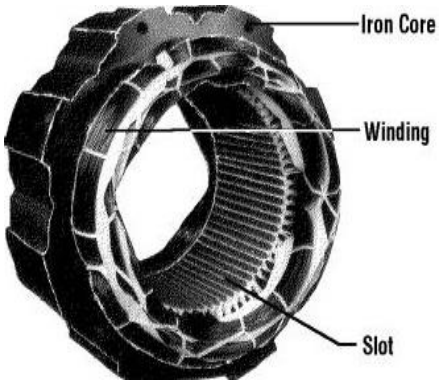

Fig. 1.3- Stator composition

b- Rotor :

The rotor is the moving part of the motor .Like the magnetic circuit of the stator, it is made up of stack of thin laminations insulated from one another, forming a keyed cylinder on the motor shaft as it is illustrated in fig.1.4.

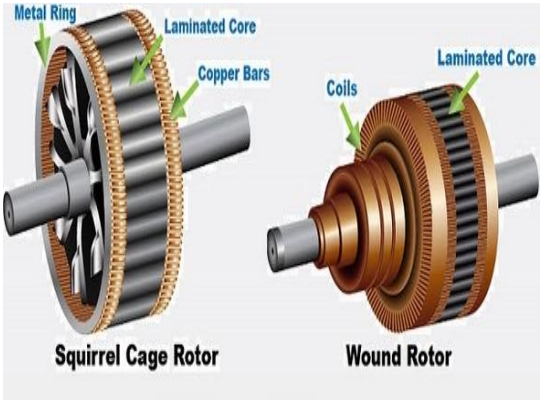

Fig. 1.4- Squirrel Cage Rotor Vs Wound Rotor

From figure 1.4, it can be seen that two different technologies can be used for this part, which separate asynchronous motors into two distinct families:

1.2.1.1 Squirrel Cage rotor :

There are several types of squirrel cage rotor. They are all designed as shown in the example in figure 1.5.

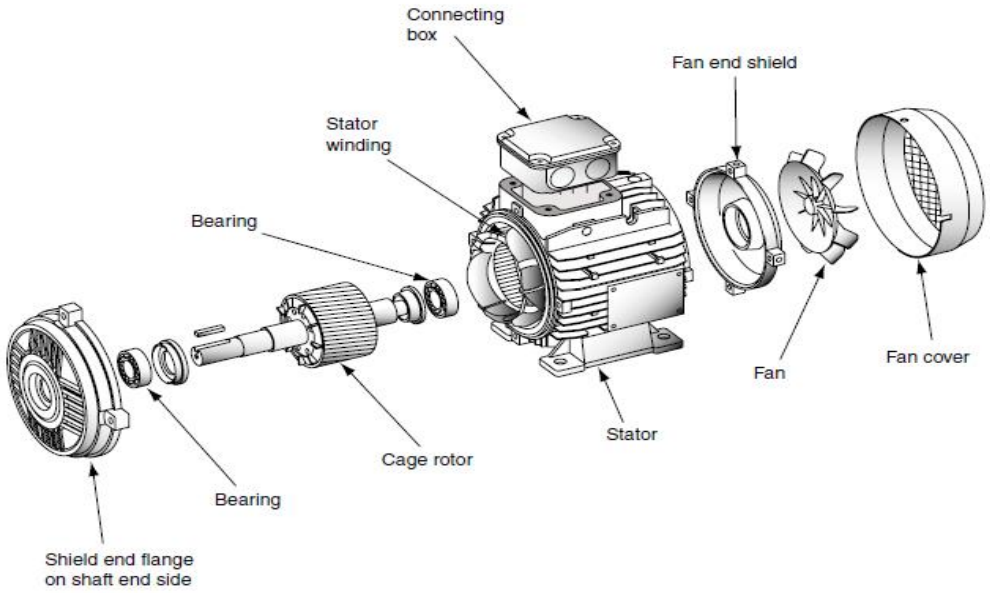

Fig.1.5-Exploded view of a squirrel cage rotor motor[03].

These different types of squirrel cage motor are:

- ✓ **Resistive squirrel-cage rotor :**

The resistive rotor mainly exists in the single cage version.The cage is closed by two resistive rings (special alloy, small cross-section, stainless steel rings,etc). These motors

have high slip at nominal torque .Their starting torque is high and the starting current is low (See fig.1.6).The efficiency of these motors is low due to the losses in the rotor. This type of motor is mainly used for application in which it is useful to have some slip in order to adapt the speed to the torque.

They are used to control the speed by modifying the voltage alone .But this application is on the decline, being increasingly replaced by frequency inverters. Although, in general, motors are self-cooled, some resistive squirrel cage motors are force-cooled (separate motorization of their fans)[03].

- ✓ **Single squirrel cage rotor :**

Conductors are placed in the holes or slots around the edges of the rotor (on the outside of the cylinder created by the stacking of the laminations) and connected at either end by a metal ring. The motor torque generated by the rotating field is applied to these conductors. To make the torque regular, the conductors are at a slight angle in relation to the motor shaft. The whole assembly resembles a squirrel cage, hence the name of this type of rotor. The squirrel cage is generally fully molded, (only very large motors are made with conductors inserted in slots). Aluminum is pressure injected and the cooling fins, which are cast in the same operation, are used for short-circuiting the stator conductors. These motors have a relatively low starting torque and the current drawn on power-up is much higher than the nominal current (see Fig.1.6). On the other hand they have low slip at nominal current. These motors are mainly used at high power to improve the efficiency of installations on pumps and fans. They are also used with frequency inverters at variable speed. The torque and current problems on starting are thus fully resolved [03].

- ✓ **Double squirrel cage rotor :**

This consists of two concentric cages, one outer, with a small cross-section, and highly resistive, and the other inner, with a large cross-section and lower resistance. At the beginning of the starting phase, when the rotor current frequency is high, the resulting skin effect causes the whole of the rotor current to flow around the outer surface of the rotor and thus in a smaller surface area of the conductors. Thus, at the beginning of the starting phase, when the rotor current frequency is high, the current only flows in the outer cage. The torque produced by the resistive outer cage is high and the current

inrush low (see Figure 1.6).At the end of the starting phase, the frequency decreases in the rotor and it is easier for the flux to flow through the inner cage. The motor then behaves very much as if it had been built with a single low resistance cage. In steady state the speed is only slightly lower than that of a single cage motor. The rotor conductors are molded into the rotor slots which are trapezoidal shape, with the small side of the trapeze located on the outer surface of the rotor [03].

The intensity of this type of rotor current varies inversely to its frequency. Thus at the beginning of the starting phase, the torque is high and the current inrush is low. In steady state the speed is more or less the same as that of a single cage motor.

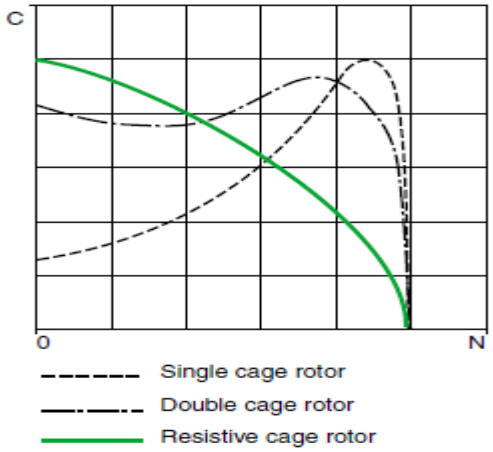

Fig. 1.6-Torque/Speed curves for the various types of cage rotor[03].

1.2.1.2 Wound rotor (slip-ring rotor) :

Identical windings to those of the stator are inserted in the slots around the outer edge of the rotor (see fig.1.7). The rotor is generally3-phase.

One end of each of the windings is connected to a common point (star connection). The free ends can be connected to a centrifugal switch or to three insulated solid copper rings that form part of the rotor. The graphite-based brushes connected to the starting device rub against these rings.

Depending on the values of the resistors inserted in the rotor circuit, this type of motor can develop a starting torque of up to 2.5 times the nominal torque.

The current on starting is more or less proportional to the torque developed on the motor shaft. This solution is now being phased out in favor of electronic solutions combined with a standard squirrel cage motor. In fact, the latter solutions resolve maintenance issues(replacement of worn rotor power supply brushes, servicing of adjustment resistors), reduce the energy dissipated in these resistors and also significantly improve the efficiency of the installation[03].

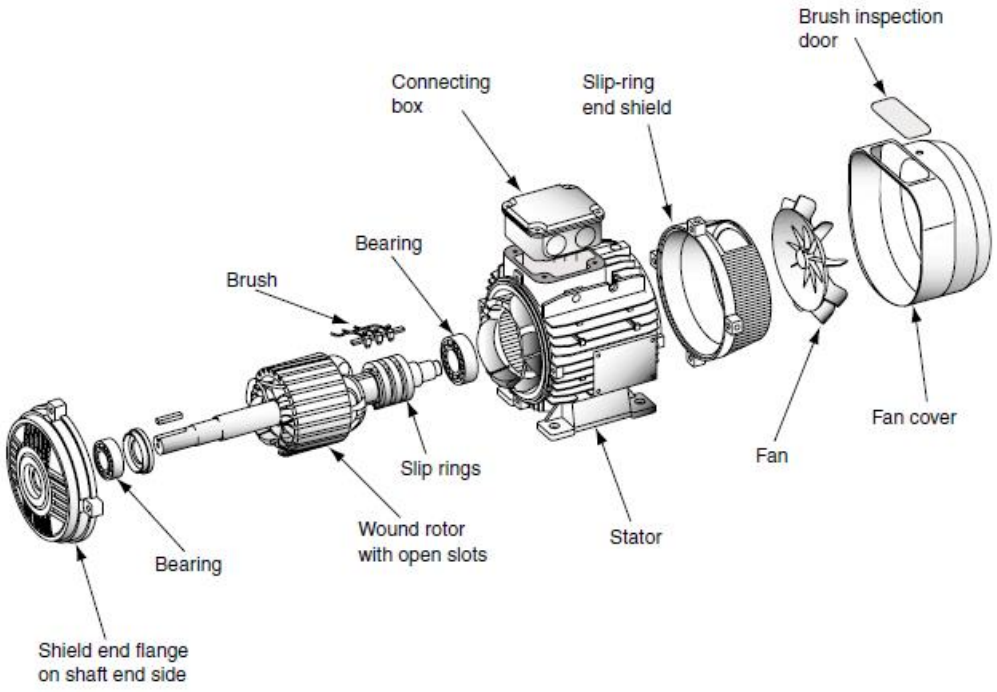

Fig. 1.7-Exploded view of a slip-ring rotor motor[03]

1.2.2. Principal of operation:

When the stator winding of an induction motor is connected to a three-phase supply , a uniform rotating magnetic field is produced therein , which induces e.m.f in the rotor that is free to rotate coaxially with the stator core with the help of ball bearings . Rotor being short circuited, either through the end rings or an external resistance, currents are produced due to this induced e.m.f. This current interacts with the rotating magnetic field to develop a torque on the rotor in the direction of the rotating magnetic field. As the rotor is free to rotate, the torque will cause it to move round in the direction of the stator field. This makes a three-phase induction motor as self-starting.

In transforming this electrical energy into mechanical energy, in an induction motor some losses occur as follows:

- Friction and windage losses [5-15%]
- Iron or core losses [15-25%]
- Stator losses [25-40%]
- Rotor losses [15-25%]
- Stray load losses [10-20%]

Full-load motor efficiency varies between 85 to 97%.

Induction motor are simpler, cheaper, and efficient .Among them squirrel-cage induction motor which is more rugged and work more efficiently compared to wound-rotor induction motor.

If supply voltage and frequency are constant, then a squirrel-cage IM runs at a constant speed which makes it suitable for use in constant speed drive. Several standard designs of squirrel-cage IM are available in the market to fulfill the requirements of different starting and running conditions of various industrial applications .These are classified as class A,class B,class C,and class D as it is shown in the table below.

Table 1.1-Comparison table of different classes of squirrel-cage Induction motor

Class	Class A	Class B	Class C	Class D
Properties	Normal starting torque ,high starting current and low operating slip	Normal starting torque ,low starting current and low operating slip	High starting torque and low starting current	High starting torque,low starting current and high operating slip
Uses	Fan ,pump load etc. where torque is low at start	For constant speed drive such as pump blower	Compressor ,conveyors, crashers, ect	For driving intermittent load, e.g punch press ect.

1.3. Mathematical model of Induction Motor

To derive the mathematical model of induction motor, its general electrical scheme is drawn in Fig.1.8 [01].

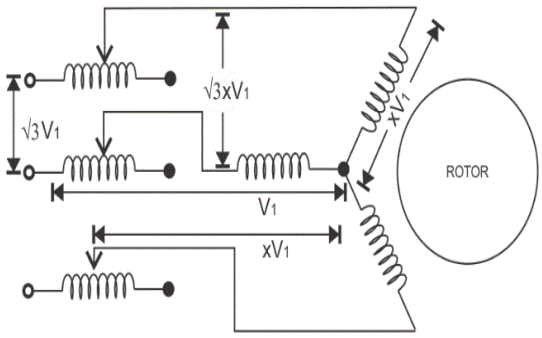

Fig. 1.8-Electric scheme of an induction motor

In order to derive the mathematical equation of a three-phase induction motor, the following assumptions are made:

- The three-phase motor is symmetrical
- Only the fundamental harmonic is considered, while the higher harmonics of the spatial field distribution and of the magneto-motive force (MMF) in the air gap are disregarded.
- The spatially distributed stator and rotor windings are replaced by a specially formed, so called concentrated coil.
- The effects of anisotropy, magnetic saturation, iron losses, and eddy currents are neglected.
- The coil resistances and reactance are taken to be constant
- In many cases, especially when considering steady state, the current and voltages are taken to be sinusoidal.

Taking into consideration the earlier-stated assumptions, the following equations of the instantaneous stator phase voltage values can be written as follows:

$$V_a = R_s i_a + \frac{d}{dt}\psi_a \tag{1.1}$$

$$V_b = R_s i_b + \frac{d}{dt}\psi_b \tag{1.2}$$

$$V_c = R_s i_c + \frac{d}{dt}\psi_c \tag{1.3}$$

Assuming that we have a three-phase balanced system meaning:

$$V_{a0} + V_{b0} + V_{c0} = 0 \tag{1.4}$$

1.3.1. D-Q model equations

By applying the a-b-c / d-q transformation the motor mathematical model becomes as follow:

- ✓ **The stator voltage differential equations:**

$$V_{sd} = R_s i_{sd} + \frac{d}{dt}\psi_{sd} - w\psi_{sq} \tag{1.5}$$

$$V_{sq} = R_s i_{sq} + \frac{d}{dt}\psi_{sq} - w\psi_{sd} \tag{1.6}$$

- ✓ **The rotor voltage differential equations:**

$$V_{rd} = 0 = R_r i_{rd} + \frac{d}{dt}\psi_{rd} - (w_s - w)\psi_{rq} \tag{1.7}$$

$$V_{rq} = 0 = R_r i_{rq} + \frac{d}{dt}\psi_{rq} - (w_s - w)\psi_{rd} \tag{1.8}$$

- ✓ **The stator and rotor flux linkages expressed in terms of the stator and rotor current space vectors:**

$$\psi_{sd} = L_s i_{sd} + L_m i_{rd} \tag{1.9}$$

$$\psi_{sq} = L_s i_{sq} + L_m i_{rq} \tag{1.10}$$

$$\psi_{rd} = L_r i_{rd} + L_m i_{sd} \tag{1.11}$$

$$\psi_{rq} = L_r i_{rq} + L_m i_{sq} \tag{1.12}$$

- ✓ **The electromagnetic torque equation expressed by utilizing space vector quantities:**

$$T_e = \frac{3}{2} P(\psi_{sd} i_{sq} - \psi_{sq} i_{sd}) \tag{1.13}$$

1.3.2. The $\alpha - \beta$ model equations

By applying the a-b-c/ $\alpha - \beta$ transformation as shown in the diagram of fig.1.9, the mathematical equations of the motor will be as follow:

$$V_\alpha + jV_\beta = \frac{2}{3}(V_a + V_b e^{\frac{j2\pi}{3}} + V_c e^{\frac{-j2\pi}{3}}) \quad (1.14)$$

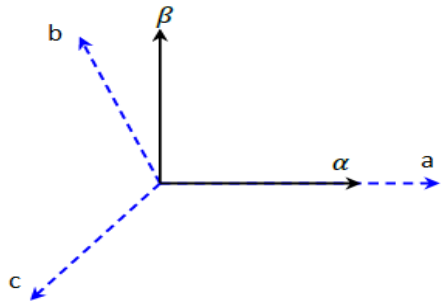

Fig. 1.9- a-b-c frame to $\alpha - \beta$ frame

The AC Induction motor model is given by the space vector form of the voltage equations. The system model defined in a two-phase stationary coordinates system attached to the stator is expressed by the following equations:

- ✓ **The stator voltage differential equations :**

$$V_{s\alpha} = R_s i_{s\alpha} + \frac{d}{dt}\psi_{s\alpha} \quad (1.15)$$

$$V_{s\beta} = R_s i_{s\beta} + \frac{d}{dt}\psi_{s\beta} \quad (1.16)$$

- ✓ **The rotor voltage differential equations :**

$$V_{r\alpha} = 0 = R_r i_{r\alpha} + \frac{d}{dt}\psi_{r\alpha} + w\psi_{r\beta} \quad (1.17)$$

$$V_{r\beta} = 0 = R_r i_{r\beta} + \frac{d}{dt}\psi_{r\beta} + w\psi_{r\alpha} \quad (1.18)$$

- ✓ **The stator and rotor flux linkages expressed in terms of the stator and rotor current space vectors :**

$$\psi_{s\alpha} = L_s i_{s\alpha} + L_m i_{r\alpha} \quad (1.19)$$

$$\psi_{s\beta} = L_s i_{s\beta} + L_m i_{r\beta} \quad (1.20)$$

$$\psi_{r\alpha} = L_r i_{r\alpha} + L_m i_{s\alpha} \quad (1.21)$$

$$\psi_{r\beta} = L_r i_{r\beta} + L_m i_{s\beta} \quad (1.22)$$

- ✓ **The electromagnetic torque equation expressed by utilizing space vector quantities :**

$$T_e = \frac{3}{2} P(\psi_{s\alpha} i_{s\beta} - \psi_{s\beta} i_{s\alpha}) \quad (1.23)$$

1.4. Different control strategies for induction motor

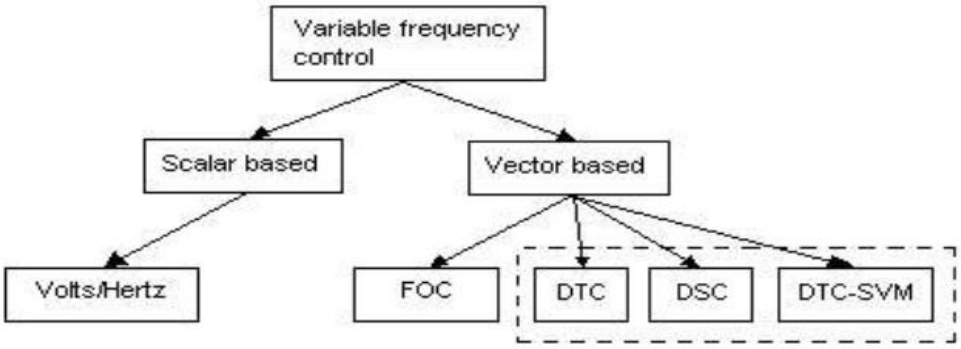

Fig. 1.10-Diagram of the different control strategies of an IM

The diagram shown in the fig. 1.10 illustrates the different control strategies existing of an induction motor [01]. These strategies can be classified into three main classes:

- Variable frequency drive
- Nonlinear control techniques
- Sensorless techniques

1.4.1. Variable frequency drive

We have two main variable frequency drive types, which are:

a- Scalar control :

Known also by "Volt/Hertz control", this technique is used to control the speed of the induction motors and all its techniques are mainly implemented through direct measurement of the machine parameters. The concept of V/f method is to keep the ratio of the stator voltage to frequency constant to maintain constant maximum available torque.

b- Vector control :

- ✓ **Field oriented control :**

Field oriented control method, known popularly as vector control is widely used in modern industrial systems. In the opposite of the scalar control, the development of FOC control scheme is based on the dynamic model of the IM which make it valid for both steady and transient states.

The field oriented control method of the motor is realized for current components in d-q rotating coordinate system.

In the field oriented control system, a stator current d-component adjusts the rotor flux in the motor, while the combination of d and q-components adjusts the motor torque. By applying the decoupling block in the particular d and q control parts the control of flux and torque can be done independently.

- ✓ **DTC:**

The direct torque control is a robust control method which is based first in estimating the machine stator flux and electric torque in the stationary reference frame from terminal measurements.

The estimated stator flux and electric torque are then controlled directly by comparing them with their respective demanded values using hysteresis comparators.

The outputs of the two comparators are then used as input signals of an optimal switching table [01].

1.4.2. Nonlinear control techniques

There are two types of nonlinear control techniques:

a- Feed-back linearization :

The feedback linearization is a transformation of nonlinear dynamics into a linear form by using state feedback. When a multiple input multiple output system is input-output linearized and decoupled, a standard linear control can be applied to simplify control design and stabilization. However this method has some limitations .For example, it is not applicable to all nonlinear systems, it only applies to the system with precise

mathematical model. While the presence of parameters uncertainty the system robustness cannot be guaranteed.

b- Sliding mode control :

The sliding mode control (SMC) is a particular type of variable structure control (VSC). Its first concepts appeared in the Soviet Union in 1950s and were later on developed by Emelyanov in 1960s .This method is designed to drive and then to constrain the system state to lie within a neighborhood of the switching surface. Its main features are the dynamics behavior of the system which may be tailored at a particular choice of switching function .This approach is independent of the object parameters which make the closed loop response becomes totally insensitive to a particular class of uncertainty in the system, which provides a very strong and inherent robustness to the resulting controllers .[12]

1.4.3. Sensorless control techniques

The measurement of speed and flux is an essential step for control design in electric drives regardless of the type of the control strategy used. The knowledge of all the components of the state vector is required in the implementation of control algorithms .However the high cost, fragility and reduced reliability of the use of sensors make it disadvantageous for them .In addition to the fact that sensors require a regular maintenance, and in some applications, it is inappropriate to install sensors due to the physical and environmental constraints .A similar situation arises when a sensor breaks down.

Thus a solution were proposed in order to overcome these difficulties and limitations .This proposition is to replace sensors with software sensors .It is known by sensorless control theory in the automatic field ,it takes a grand part in this domain .The software sensors are called estimators or observers .The objective of this sensorless control for electrical machines is to estimate mechanical speed and torque or flux vector and its position .The speed sensorless control for ac drives has taken a big attention in industry application in the past decade, since it can reduce the cost and avoid the difficulty of installing mechanical sensors.

1.5. Conclusion

In this first chapter, a background about induction motor was presented, its construction principle of operation, mathematical model and its different control techniques used.

In the next chapter, basics about the direct torque control for an induction motor will be discussed through this section.

2.1. Introduction:

In mid 1980s, innovative studies have been carried by Depenbrock [06],[07] and by both Isao Takahashi and Toshihiko Noguchi[10].Those studies proposed a new concept of control for A.C machine which is the direct torque control.

DTC of an induction motor has been successful because it explicitly considers the inverter stage and uses few machine parameters, while being more robust to parameter uncertainty than field-oriented control [04].

Therefore there are lots of questions which need to be investigated further in this aspect.

This chapter illustrates the theoretical basics needed concerning the conventional D.T.C for induction motor drives.

2.2. Model of induction motor dedicated for direct torque control

The following equations express the dynamic equation's model of the induction dedicated for direct torque control expressed in the stationary frame (α, β) :

$$\frac{di_{s\alpha}}{dt} = -\left(\frac{R_s}{\sigma L_s} + \frac{R_r}{\sigma L_r}\right) i_{s\alpha} - w_r i_{s\beta} + \frac{R_s}{\sigma L_s L_r} w_{s\alpha} - \frac{w_r}{\sigma L_r} w_{s\beta} + \frac{1}{\sigma L_s} u_{s\alpha} \tag{2.1}$$

$$\frac{di_{s\beta}}{dt} = -\left(\frac{R_s}{\sigma L_s} + \frac{R_r}{\sigma L_r}\right) i_{s\beta} - w_r i_{s\alpha} + \frac{R_s}{\sigma L_s L_r} w_{s\beta} - \frac{w_r}{\sigma L_r} w_{s\alpha} + \frac{1}{\sigma L_s} u_{s\beta} \tag{2.2}$$

$$\begin{cases} \frac{d\psi_{s\alpha}}{dt} = u_{s\alpha} - R_s i_{s\alpha} \\ \frac{d\psi_{s\beta}}{dt} = u_{s\beta} - R_s i_{s\beta} \end{cases} \tag{2.3}$$

Where: $\sigma = 1 - \frac{M_{sr}}{L_s L_r}$ is the Blondel's coefficient.

2.3. Two-level voltage source inverter VSI model

Figure 2.1 represents a two-level three legs voltage inverter fed an induction motor.This motor is supposed to be a star-connected three phase balanced load.

The type of the used switches depends on the power of the inverter and switching frequency. In the most applications, IGBT transistors with anti-parallel diodes are used.

The output phase voltages are produced by a DC link voltage V_{dc} which is provided by a rectifier, battery pack or any another DC source [9].

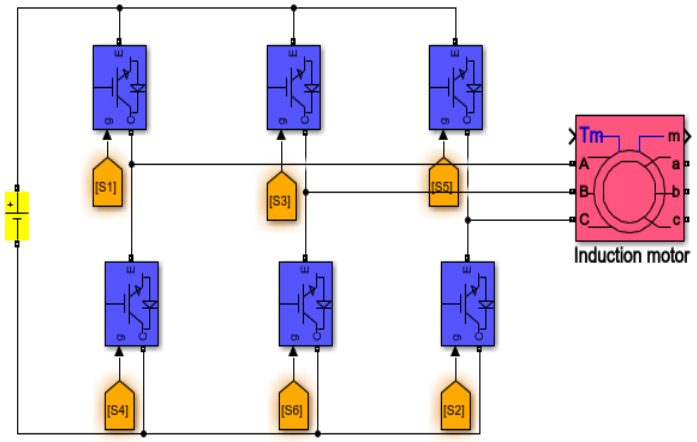

Fig. 2.1- Three phase VSI fed an induction motor.

The six switches are divided into two groups:

- upper three switches as positive group (i.e. S_1, S_2, S_3)
- And lower three as negative group of switches (i.e. S_4, S_5, S_6).

There are two possible gating patterns to the switches which are:

- 180° conduction mode,
- And 120° conduction mode.

In each pattern the gating signals are applied and removed at an interval of 60° of the output voltage waveform. In 180° mode three switches are on at a time, two from positive group and one from negative group and vice versa, each switch conducts for 180° of a cycle. In 120° mode each switch conduct for 120° in one cycle and two switches remain turn on at a time, one from positive group and one from negative group. But no two switches of the same leg should be turned on simultaneously in both cases as this condition would short circuit the dc source [13].

The inverter's control bases on the logic values S_i where:

$$S_i = 1 \text{ , } T_i \text{ is ON and } \overline{T}_i \text{ is OFF .}$$

$$S_i = 0, T_i \text{ is OFF and } \overline{T}_i \text{ is ON .}$$

With i=a ,b ,c.

The voltage vector is generated by the following equation [12]:

$$V_s = \sqrt{\frac{2}{3}V_{dc}}\,[S_a + S_b e^{j\frac{2\pi}{3}} + S_c e^{j\frac{4\pi}{3}}] \qquad (2.4)$$

Where: V_{dc} is the DC link voltage

The standard three-phase VSI topology has eight valid switching states which are given in table 2.1.Two are zero voltage states(V_0, V_7)which produce zero ac line voltage and in this case ,either through the upper or lower components, the ac currents free wheel. The remaining six states (V_1, V_2 …..V_6) are active vectors which produce non-zero ac output voltages. The inverter switches from one state to another in order to generate a given voltage waveform.

Table 2.1-Switching state of a three phase V.S.I.

State	S_a	S_b	S_c	Vector
0	0	0	0	V_0
1	1	0	0	V_1
2	1	1	0	V_2
3	0	1	0	V_3
4	0	1	1	V_4
5	0	0	1	V_5
6	1	0	1	V_6
7	1	1	1	V_7

These eight switching states are illustrated as space vectors in figure 2.2.

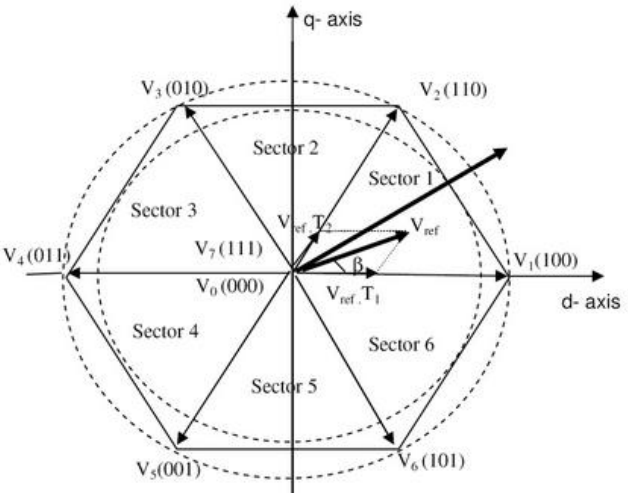

Fig. 2.2- VSI voltage vectors in the complex plane [10].

2.4. Principles of Direct torque control

A simplified scheme of the direct torque control is presented in figure 2.3.

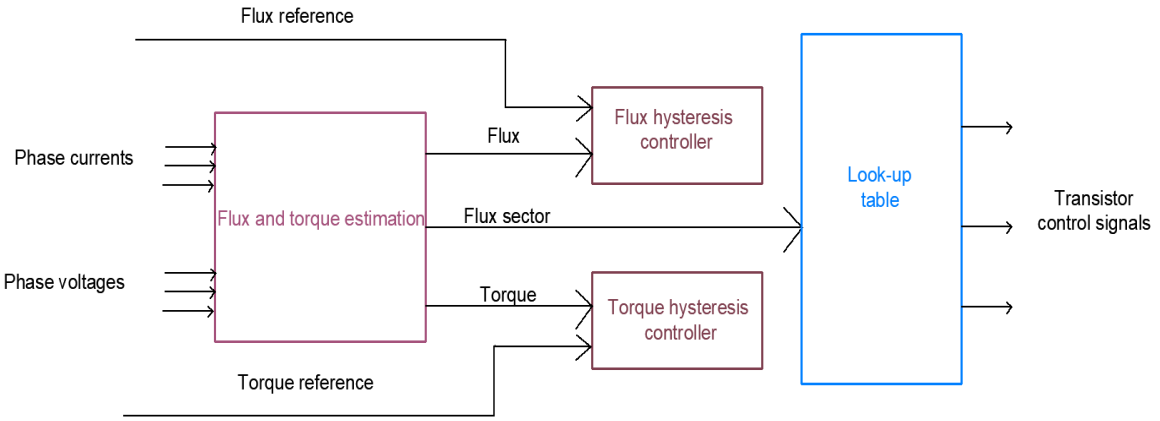

Fig. 2.3- A simplified block diagram of direct torque control.

From figure 2.3, it can be noticed that based on the measurements of both the stator voltage and current, the stator flux vector and the developed torque are calculated. Then the magnitude of the stator flux is compared in the flux control loop with reference value, whereas the developed torque is compared with the reference torque in the torque control loop.

The flux and torque errors, are applied to respective bang-bang controllers, whose characteristics are shown in figure 2.4 and figure 2.5.Consequently, the flux and torque controllers' output signals along with the flux sector are inputs to the voltage vector table which generates the appropriate control voltage vector are input to the voltage vector table which generates the appropriate control voltage vector in other words they will generate the consecutive inverter switching states by the use of the look-up table. The inverter output voltage are then input to the d-q model of the induction motor.

2.5. D.T.C global scheme

A global scheme of the algorithm of the direct torque control technique is shown in figure 2.4.

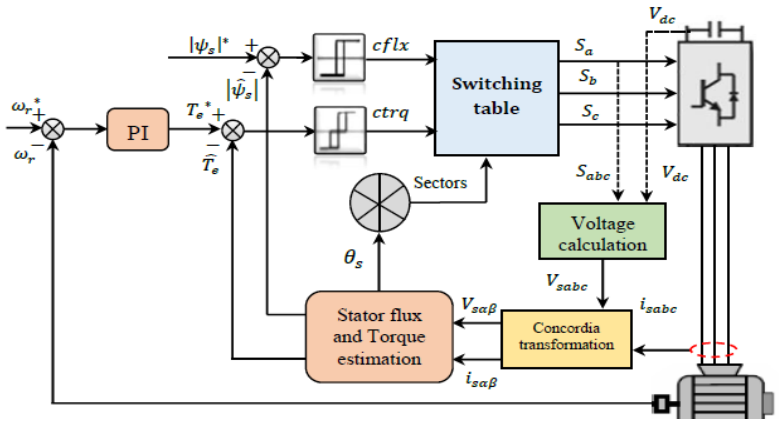

Fig. 2.4- Global schematic for direct torque control.

The DTC global scheme can be divided into the following sub-units:

2.5.1. Control of stator flux and electromagnetic torque

- ✓ **Control of stator flux :**

Based on the IM model in stationary frame, the stator flux equation can be expressed as follows:

$$\frac{d\psi_s}{dt} = V_s - R_s i_s \tag{2.5}$$

And:

$$\psi_s(t) = \int_0^{T_z} (V_s - R_s i_s) dt + \psi_s(0) \tag{2.6}$$

Where $\psi_s(0)$ is the flux vector at the instant t=0s .

By applying a non-zero vector in T_z sampling period, the stator resistance voltage drop i.e. $R_s i_s$ compared to V_s for high speed regions can be neglected. Thus, equation (2.6) can be written as:

$$\psi_s(t) \approx V_s T_z + \psi_s(0) \tag{2.7}$$

The relation between stator voltage and the stator flux change can be established as:

$$\Delta\psi_s = \psi_s(t) - \psi_s(0) = V_s T_z \tag{2.8}$$

The equation (2.8) means that the stator flux can be changed by the application of stator voltage during a timeT_z. The stator flux vector's extremity moves in direction given by the voltage vector and making a circular trajectory (see figure 2.5) [13].

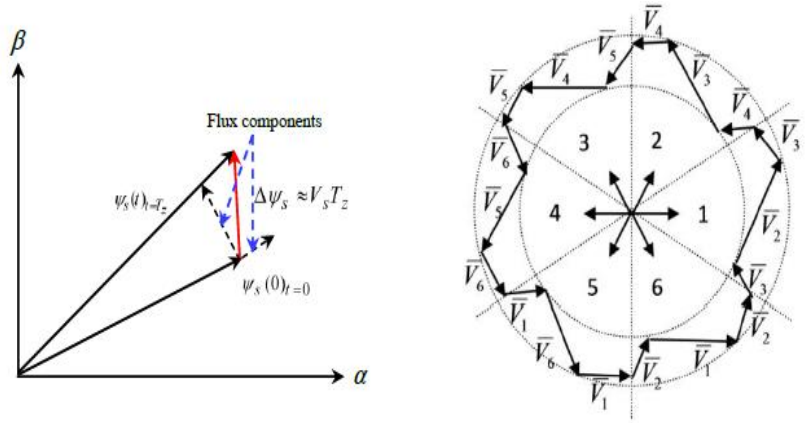

Fig. 2.5- Evolution of stator flux vector in the complex [13].

A two-level hysteresis comparator is used for flux regulation. It allows to drop easily the flux vector extremity within the limits of the two concentric circles with close radius, as shown in figure 2.6. The choice of the hysteresis bandwidth h_{ψ_s} depends on the switching frequency of the inverter.

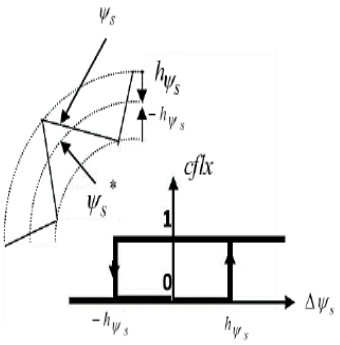

Fig. 2.6- Two level hysteresis comparator for stator flux control.

The logical outputs of the flux controller are defined as:

$$\begin{cases} \text{Cflx} = 1 & \text{if } \Delta\psi_s > \text{h}_{\psi_s} \\ \text{Cflx} = 0 & \text{if } \Delta\psi_s \leq \text{h}_{\psi_s} \end{cases} \tag{2.9}$$

h_{ψ_s} is the hysteresis band of stator flux

The stator flux error is defined by the difference between reference value and the actual estimated value:

$$\Delta\psi_s = /\Delta\psi_s^*/ - /\psi_s/ \tag{2.10}$$

- ✓ **Control of electromagnetic torque :**

During one sampling period, the rotor flux vector is supposed invariant. The torque of Induction Motor can be expressed in terms of stator and rotor flux vectors as follows:

$$T_e = p\frac{M_{sr}}{\sigma L_s L_r}\psi_s.\psi_r \tag{2.11}$$

$$|T_e| = p\frac{M_{sr}}{\sigma L_s L_r}|\psi_s| * |\psi_r| sin(\delta) \tag{2.12}$$

From equation (2.11), it is clear that the electromagnetic torque is controlled by the stator and rotor flux amplitudes. If those quantities are maintaining constant, the torque can be controlled by adjusting the load angleδ.

The torque regulation can be realized using three-level hysteresis comparator as shown in figure 2.7 and can be used for one rotation sense.

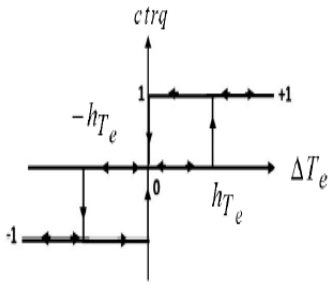

Fig. 2.7- Three level hysteresis comparator for electromagnetic torque control.

The logical outputs of the torque controller are defined as:

$$\begin{cases} ctrq = 1 & if\ \Delta T_e > h_{T_e} \\ ctrq = 0 & if\ -h_{T_e} \le \Delta T_e \le h_{T_e} \\ ctrq = -1 & if\ \Delta T_e < -h_{T_e} \end{cases} \quad (2.13)$$

where h_{T_e} is the hysteresis band torque.

The torque error is defined by the difference between the references values of the torque and the actual estimated values:

$$\Delta T_e = T_e^{*} - T_e \quad (2.14)$$

2.5.2. Estimation of stator flux and electromagnetic torque

2.5.2.1. Stator flux estimation

The estimation of the stator flux is usually done by the integration of the back-emf (electromotive force). The stator flux components can be expressed using stator voltages and currents in the stationary reference frame (α, β) by :

$$\begin{cases} \psi_{s\alpha} = \int_0^t (V_{s\alpha} - R_s i_{s\alpha}) dt \\ \psi_{s\beta} = \int_0^t (V_{s\beta} - R_s i_{s\beta}) dt \end{cases} \quad (2.15)$$

The stator flux magnitude and flux angle can be computed as:

$$|\psi_s| = \sqrt{\psi_{s\alpha}^{\,2} + \psi_{s\beta}^{\,2}} \quad (2.16)$$

$$\theta_s = \tan^{-1}(\frac{\psi_{s\beta}}{\psi_{s\alpha}}) \tag{2.17}$$

By applying Concordia transformation on the output voltage of the three-phase VSI, the stator voltage components ($V_{s\alpha}, V_{s\beta}$) will be as follow:

$$\begin{pmatrix} V_{s\alpha} \\ V_{s\beta} \end{pmatrix} = \begin{pmatrix} 1 & -1/2 & -1/2 \\ 0 & \sqrt{3}/2 & -\sqrt{3}/2 \end{pmatrix} * \begin{pmatrix} V_{sa} \\ V_{sb} \\ V_{sc} \end{pmatrix} \tag{2.18}$$

The output voltages of VSI which are the input stator voltages of the IM are given by:

$$\begin{cases} V_{sa} = \frac{V_{dc}}{3}(S_a - S_b - S_c) \\ V_{sb} = \frac{V_{dc}}{3}(2S_b - S_c - S_a) \\ V_{sc} = \frac{V_{dc}}{3}(2S_c - S_a - S_b) \end{cases} \tag{2.19}$$

The stator currents components ($i_{s\alpha}$, $i_{s\beta}$) can be obtained also by applying the Concordia transformation on the measured currents:

$$\begin{cases} i_{s\alpha} = \sqrt{\frac{2}{3} i_{sa}} \\ i_{s\beta} = \frac{1}{\sqrt{2}}(i_{sb} - i_{sc}) \end{cases} \tag{2.20}$$

2.5.2.2. Electromagnetic torque estimation

The produced electromagnetic torque of the IM motor can be determined using the cross product of the stator quantities (i.e, stator flux and stator currents).

The torque formula is expressed as following:

$$T_e = p(\psi_{s\alpha} i_{s\beta} - \psi_{s\beta} i_{s\alpha}) \tag{2.21}$$

2.5.3. Switching table construction and control algorithm design Sector calculator

There are six sectors, each $\frac{\pi}{3}$ angle wide. To determine the operating sector of the motor, the flux vector angle $\emptyset_s$ can be calculated as:

$$\emptyset_s = \tan^{-1}(\frac{\psi_{qs}}{\psi_{ds}}) \quad (2.22)$$

Depending on the angle of the flux vector, the correct sector S_{1-6} is chosen.

- **Six sectors switching table :**

To maintain a decoupled control, pair of hysteresis comparators for both the stator flux and the torque are used. These hysteresis controllers receive the stator flux and torque errors as inputs. Then, this controller outputs determine the appropriate voltage vector selection based on the switching table. However the choice of voltage vector is not only depending on the output of hysteresis controllers, but also on the position of stator flux vector. Thus, the circular stator flux vector trajectory will be divided into six symmetrical sectors as shown in figure 2.8 where:

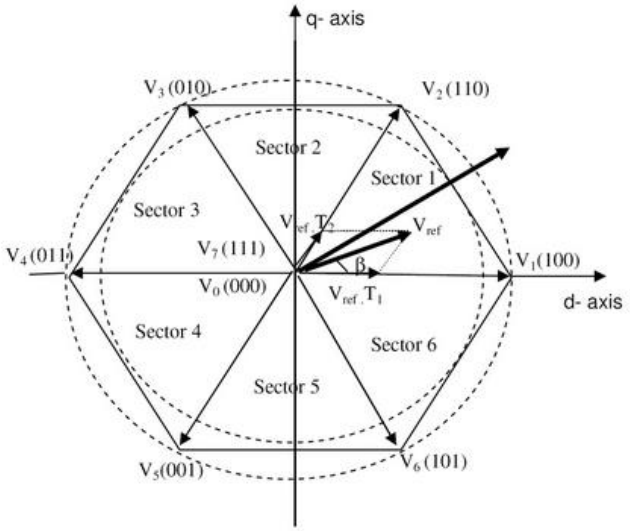

Fig. 2.8- Stator flux vector trajectory.

For stator flux vector laying in sector I we will have [12]:

- If V_i is selected, ψ_s increases and T_e increases.
- If V_{i-1} is selected, ψ_s increases and T_e decreases.
- If V_{i+2} is selected, $\psi_s$decreases and T_e increases.
- If V_{i-2} is selected, ψ_s decreases and T_e decreases.

For each sector, the vectors (V_i , V_{i+3}) are not considered because both of them can increase or decrease the torque in the same sector according to the position of flux vector on the first or the second sector. If the zero vectors V_0 and V_7 are selected, the stator flux will stop moving

and its magnitude will not change, the electromagnetic torque will decrease, but not as much as when the active voltage vectors are selected.

The resulting look-up table for DTC which was proposed by Takahashi is presented in table 2.1.

Table 2.2- Look-up table for basic direct torque.

Error	Sectors	I	II	III	IV	V	VI
Cflx=1	Ctrq=1	V_2	V_3	V_4	V_5	V_6	V_1
	Ctrq=0	V_7	V_0	V_7	V_0	V_7	V_0
	Ctrq=-1	V_6	V_1	V_2	V_3	V_4	V_5
Cflx=0	Ctrq=1	V_3	V_4	V_5	V_6	V_1	V_2
	Ctrq=0	V_0	V_7	V_0	V_7	V_0	V_7
	Ctrq=-1	V_5	V_6	V_1	V_2	V_3	V_4

2.5.4. Speed regulation in DTC strategy

One of the advantages of the D.T.C is that for the implementation of the induction flux and torque control no speed sensor is needed [14]. This can classify DTC as a speed sensorless strategy for many industrial applications .Otherwise, to achieve an adjustable speed control, a speed controller is necessary in order to regulate the speed and thus to generate the reference of electromagnetic torque.

Proportional-integral-differential (PID) controllers to be exact the PI controllers are the most widely used controllers for the regulation. The regulation using a PI is done by comparing the speed reference signal to the actual measured speed value .This comparison error is the input of the PID controller.

The most commonly used PI is the anti-windup controller. This proportional integrator controller enhances the speed control performance by cancelling the windup phenomenon which is caused by the saturation of the pure integrator.

Figure 2.9 shows the speed anti-windup PI controller diagram block.

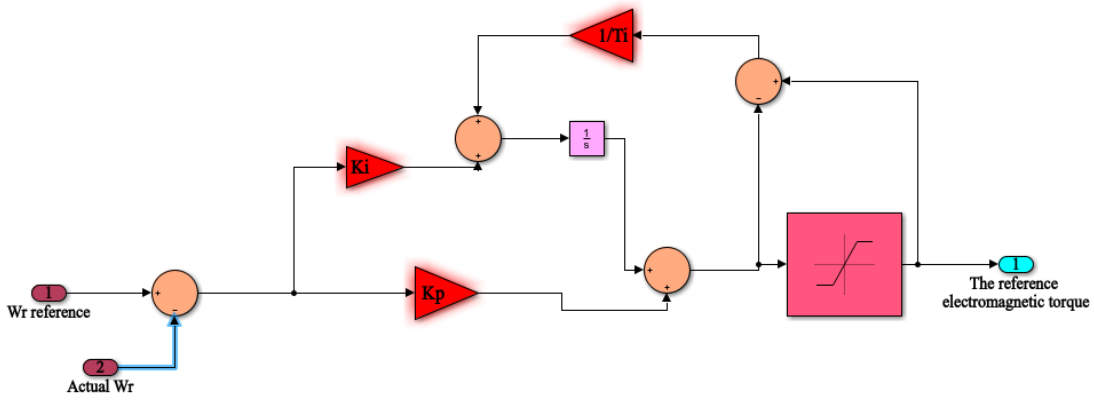

Fig. 2.9- Speed anti-windup PI controller.

This strategy consists on the correction of the integral action based on the difference between the control signal and the saturation limit.

The difference value is passed through a gain block (tracking time constant T_i) before arriving as feedback to the integrator.

2.6. Conclusion

This chapter covered the theoretical background about the direct torque method used in order to control the induction motor.

This method is called a robust control method as it is independent of the motor parameter, it only need the stator resistance.

In the next chapter, the simulation results' of all these mathematical equations which were used in order to build the algorithm of the Direct torque control for an induction motor are displayed.

Introduction:

This chapter presents the simulation results of the conventional D.T.C for induction motor using MATLAB/ Simulink software V2018. This simulation has been conducted for a three-phase 1.8kW squirrel-cage induction motor.

Simulation description:

The mathematical equations of the algorithm of the D.T.C discussed in the previous chapter have been modeled using Simulink. Figure 3.1 illustrates the proposed general block diagram of the D.T.C model using Simulink.

In this simulation the performance of the motor is first checked out for half a period for no load condition and then for a load torque of 10N.m application at t=0.5 s .The technical characteristics of the 1.8kW squirrel-cage induction motor used are drawn in table A.1.1.

The simulation covered both the starting up and the steady states operation of the controlled motor without/with load.

The chosen bandwidths of the hysteresis controllers are:

- ✓ **For the flux :** +/- 0.005Wb ,
- ✓ **For the electromagnetic torque:** +/- 0.05N.m.

Furthermore, the speed response is compared to a speed reference of 100 radian/seconds.

The block diagram illustrated in Figure 3.1 presents the following physical parameters: the flux estimation, torque estimation, the speed control loop, in addition the power supply circuit of the boost that allows to boost the 24V which consists a two 12 V lead acid batteries connected in series up to 400V in order to feed the inverter and thus the induction motor.

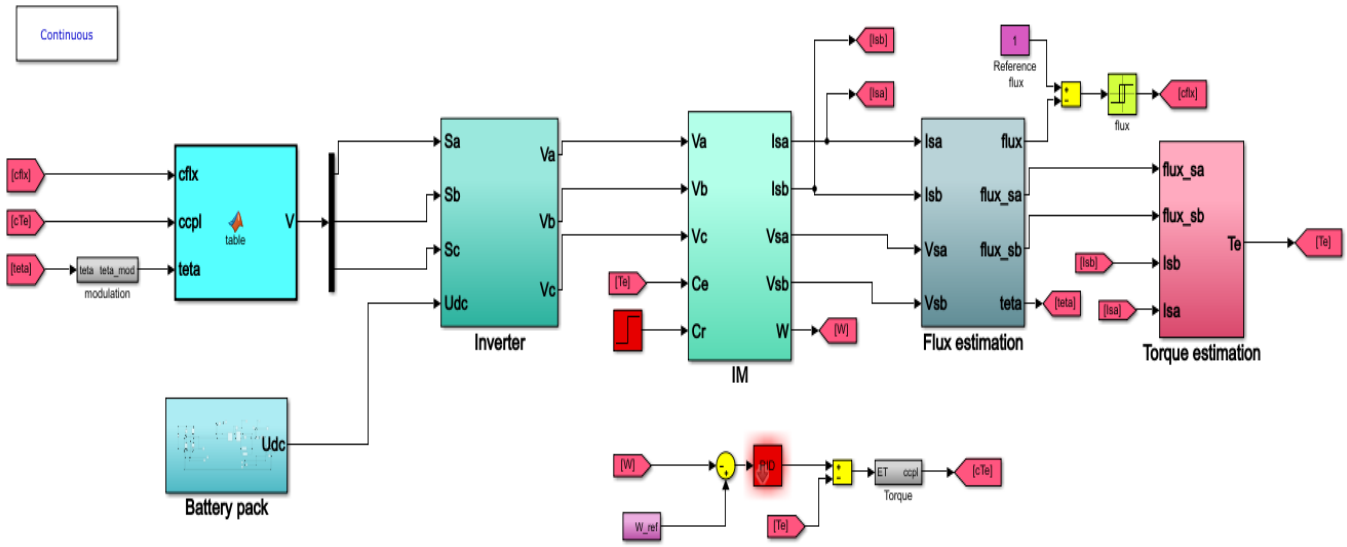

Fig.3.1- A general Simulink block diagram of the proposed D.T.C

Figure 3.2 presents the simulink block diagram of the mathematical model of an induction model as modeled in chapter 01 .

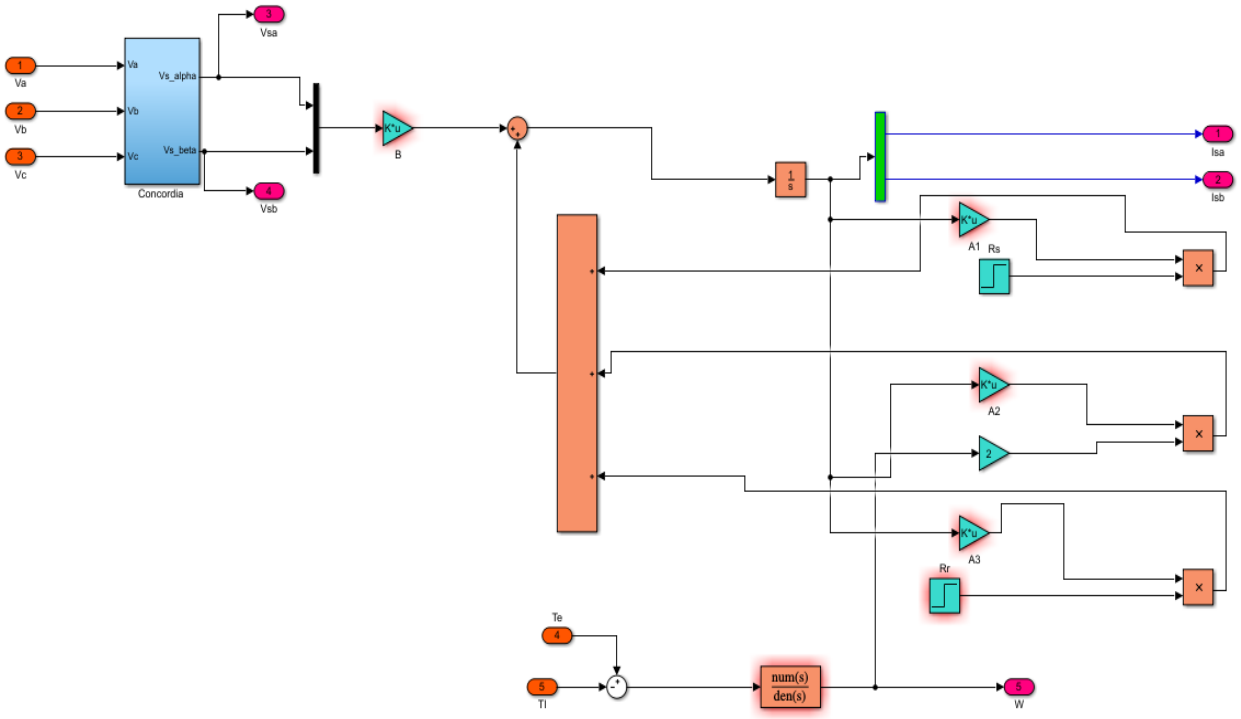

Fig. 3.2- Induction motor block diagram simulink

Figure 3.3 shows the topology of the proposed D.C to D.C isolated high power boost converter. The main component of this circuit is the transformer, a high switching frequency transformer (50 kHz) with a turn ratio of 24V/600V. This transformer is characterized by high current in the primary.

The switching on and off of the Mosfet in the low voltage side is done by the triggering signals from the comparator between the repetitive triangular sequence and a step of an amplitude of 2 and the other one of the PID. So whenever the output voltage is less than the required one , the boost try to step up in order to reach the reference value of 400V .

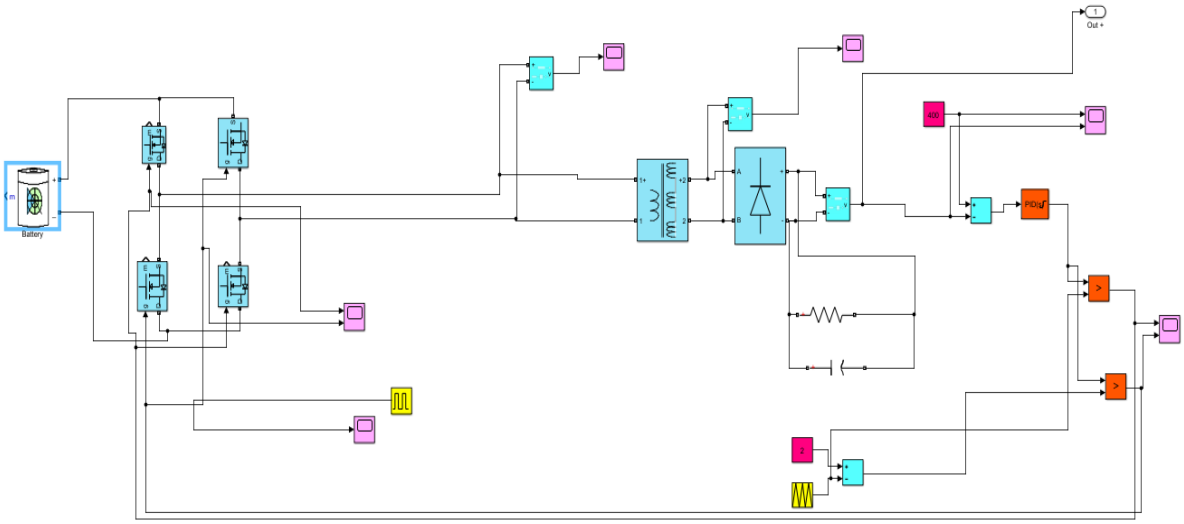

Figure 3.3: Boost Simulink block diagram of the boost

Results:

The different simulation results obtained are shown in the figures below.

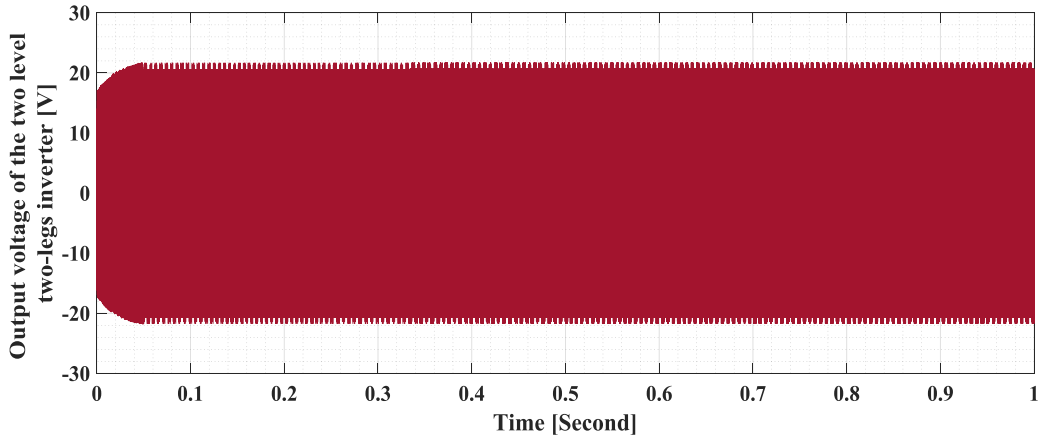

Fig. 3.4- The two level two-leg output voltage

Figure 3.4 represents the output voltage generated at the two level two-leg inverter. It is seen that the amplitude of this AC signal is 24V which is the amplitude of the two 12V lead acid batteries connected in series. These two batteries are used as our main power source.

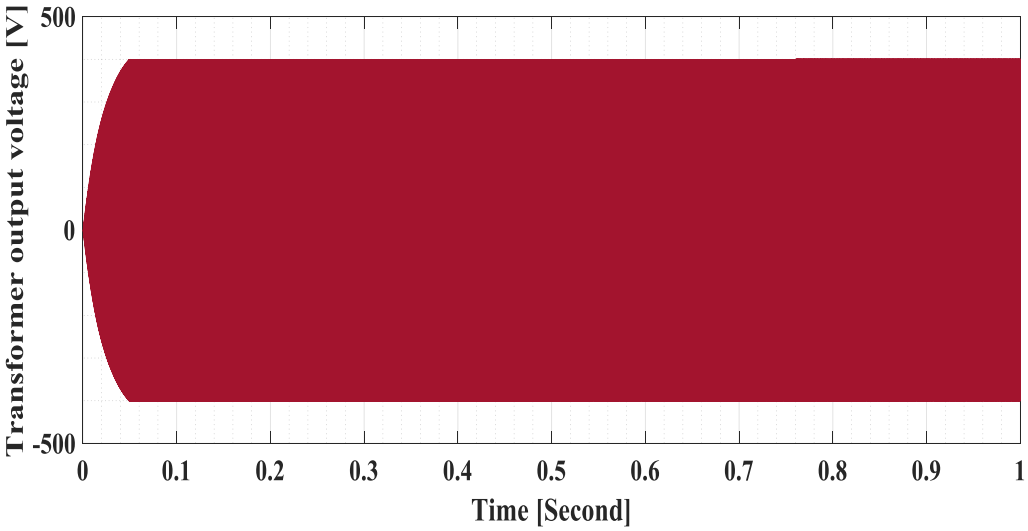

Fig. 3.5- Transformer output voltage

Figure 3.5 represents the secondary voltage of the transformer .It is seen that the value of the voltage is 400 V AC as the used transformer turn ratio is 24/600.

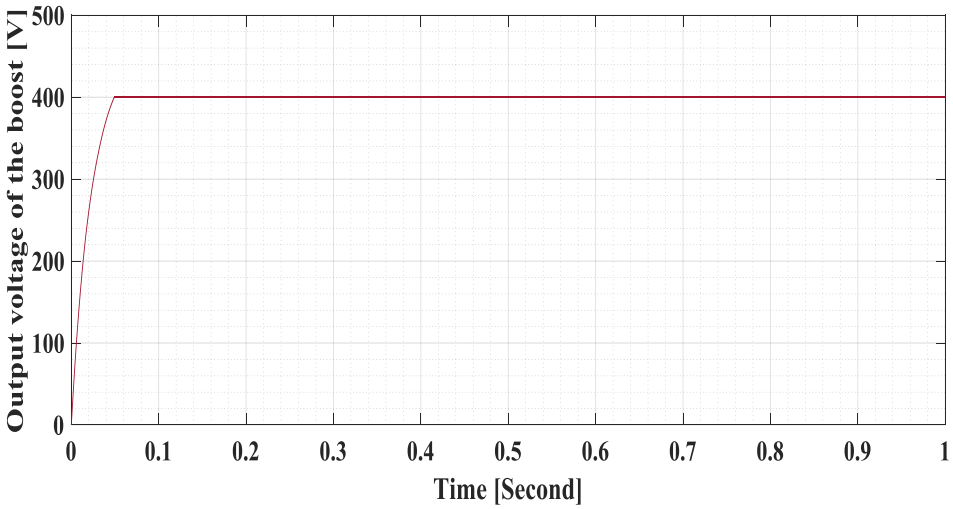

Fig. 3.6- High power boost output voltage

Figure 3.6 depicted the output voltage of the high power boost which is 400V DC. Meaning that this proposed topology of boost have been simulated successful as the

Obtained regulated output voltage satisfies the needed voltage requirement for the inverter fed the 1.8kW induction squirrel cage motor.

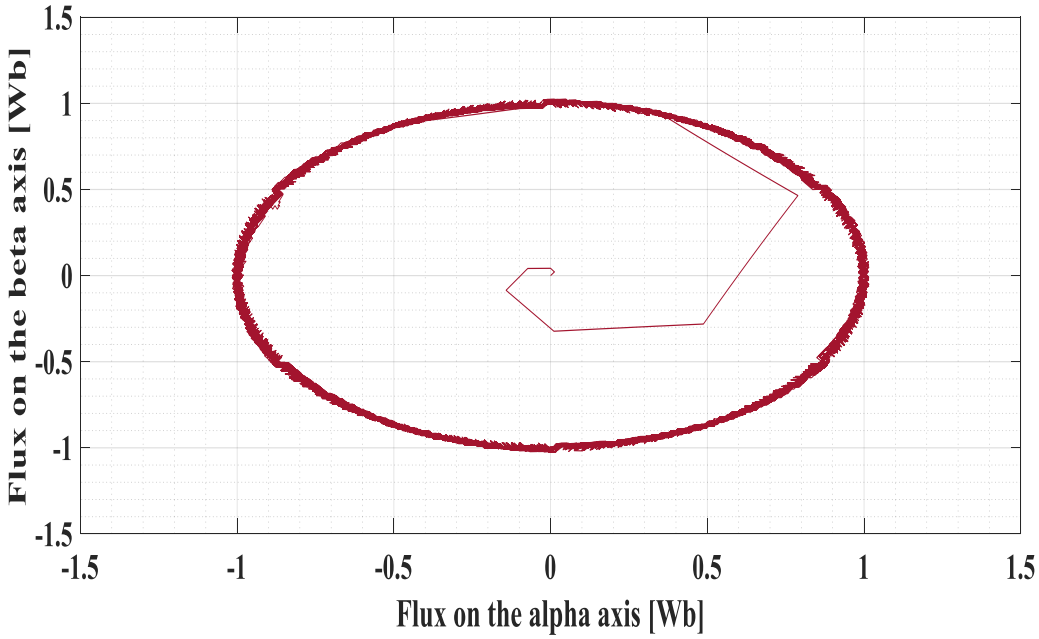

Fig. 3.7- Flux circular trajectory

Figure 3.7 of the circular trajectory represents the plotting of the flux beta component in function of the flux alpha component.

It is noticed that the circle takes a few steps before reaching the reference value of 1Wb.

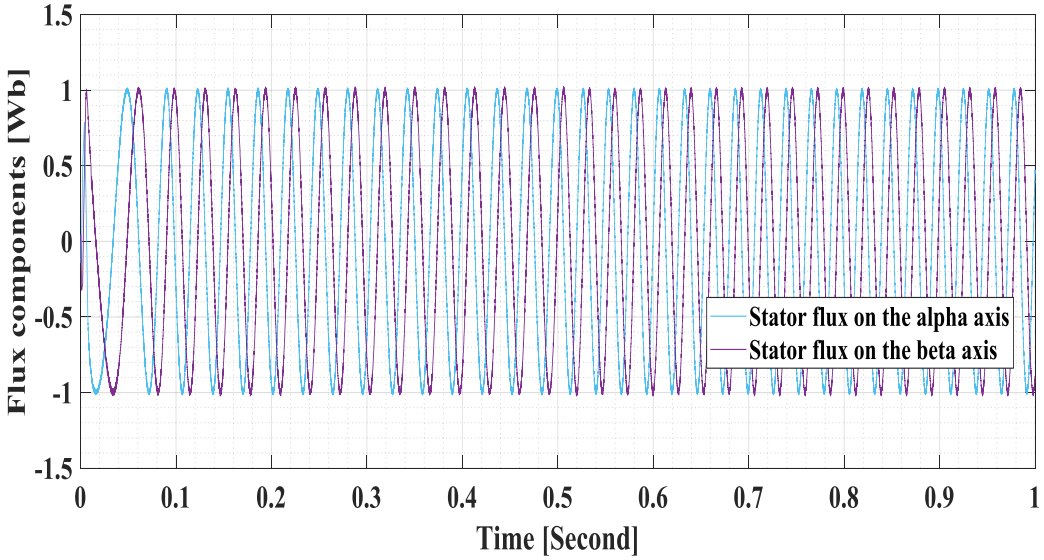

Fig. 3.8- Flux components

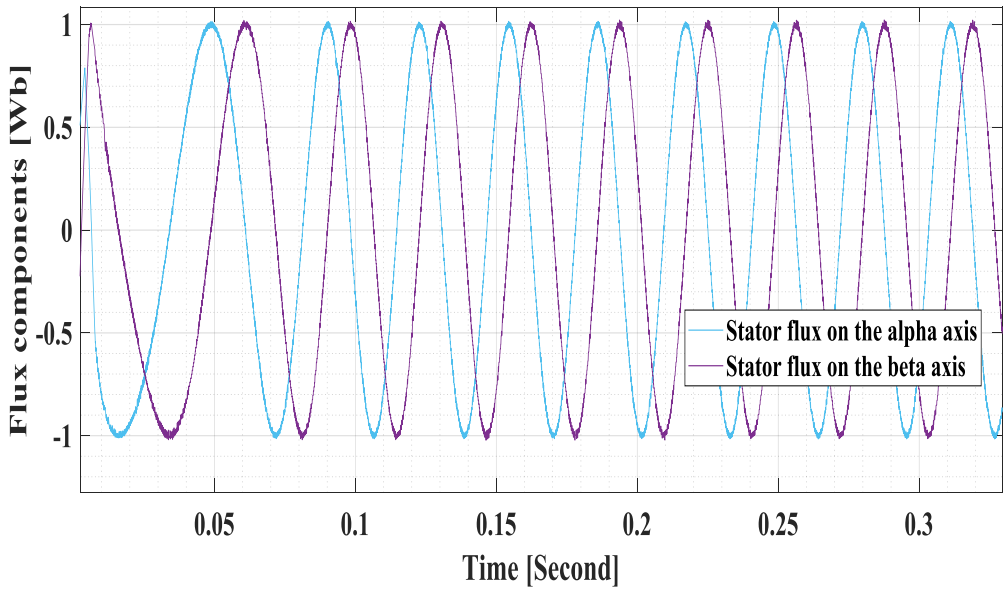

Fig. 3.9- A zoom on the Flux components

Both figures 3.8 and 3.9 represent the flux components curves and their zoom respectively. These figures show that the stator flux on the alpha axis and the one on the beta axis are sine waves of magnitude of 1Wb. It is also noticed that the phase shift between these two sine waves is 120°.

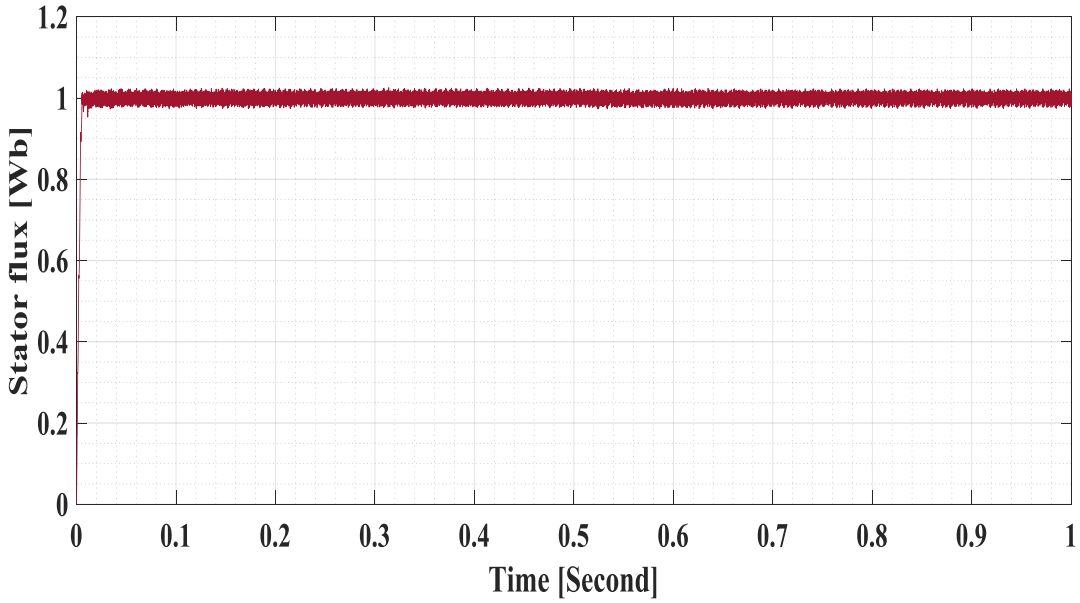

Fig. 3.10- Stator flux

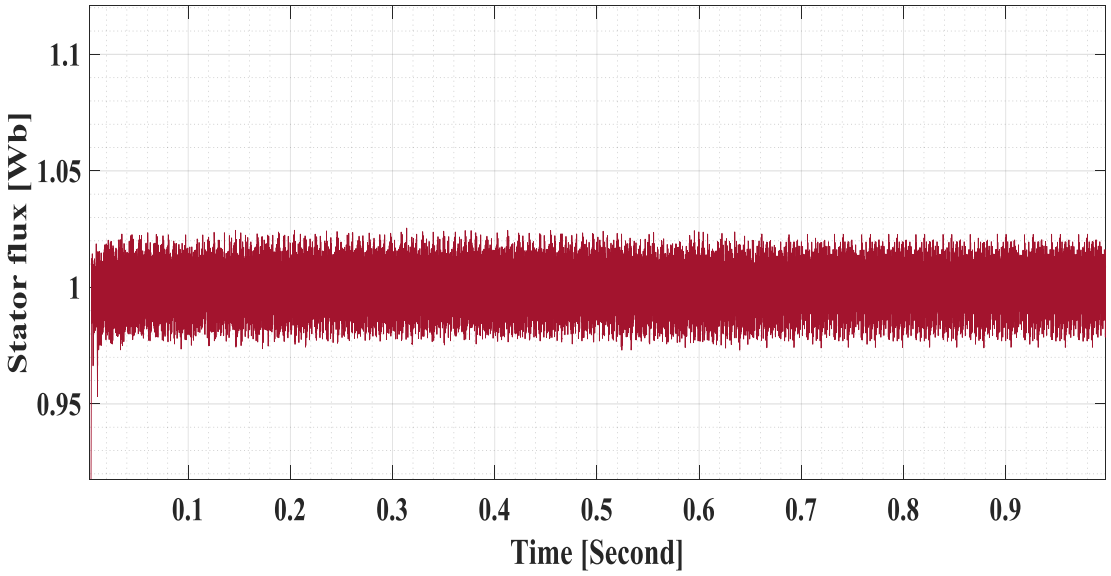

Fig. 3.11- A zoom on the stator flux

It is noticed from both figures 3.10 and 3.11 which represent the stator flux magnitude and its zoom respectively that the output flux of the hysteresis controller lies in the neighborhood of the reference value which is 1Wb .

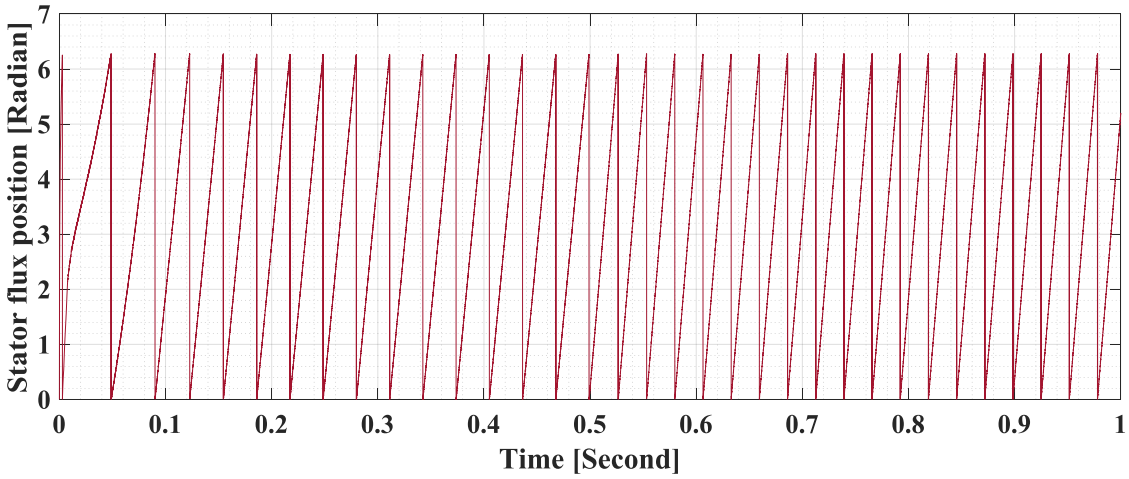

Figure 3.12 : Flux position

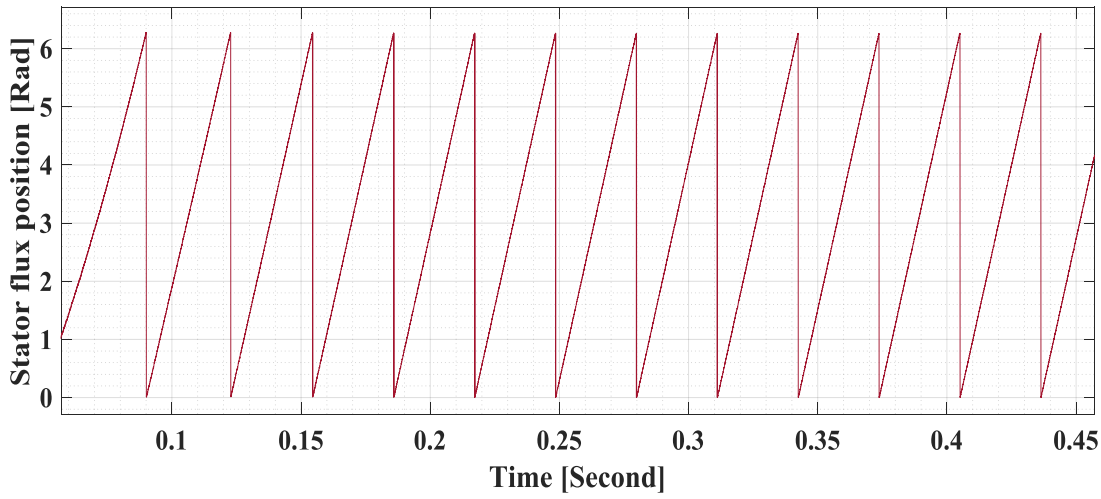

Fig. 3.13- A zoom on the flux position curve

From figures 3.17 and 3.18, it is noticed that the flux curve has a repetitive triangular form .

It is noticed from the figures of the stator flux both of the magnitude and position 3.10-3.13 that the change in motor torque doesn't have control over fluxes.

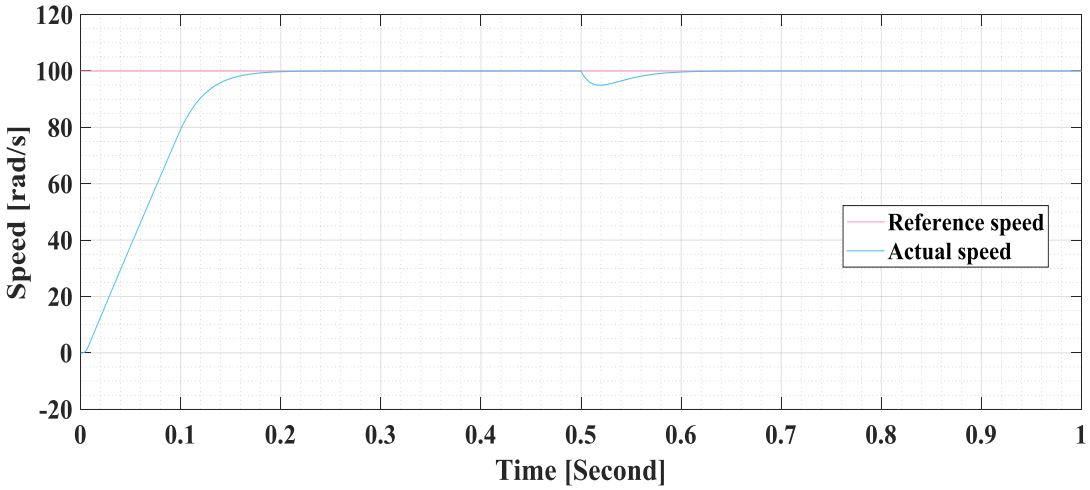

Fig. 3.19- Rotor speed

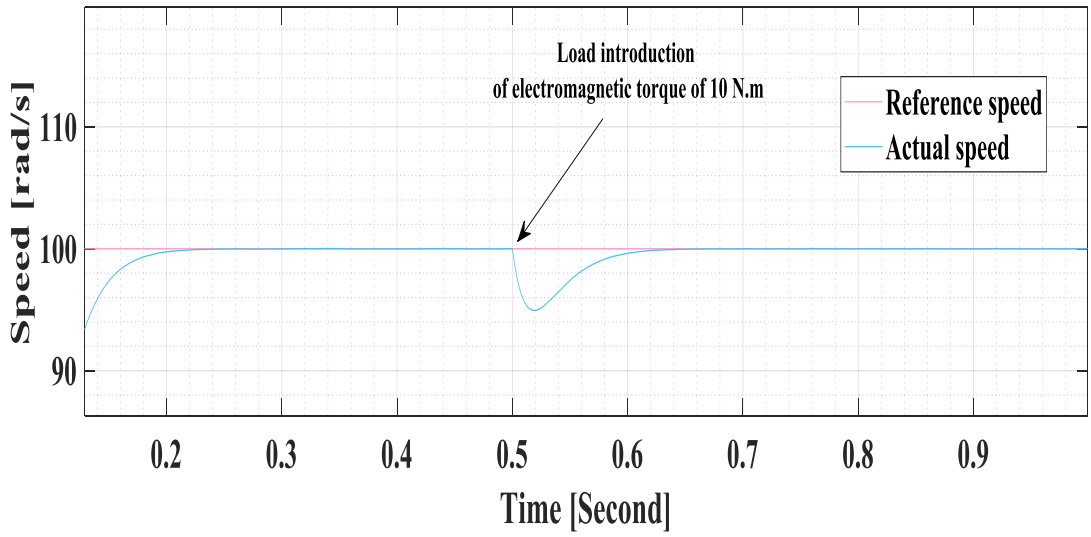

Fig. 3.14- A zoom on the rotor speed

The rotor speed of the induction motor compared with a reference speed step of 100 rad/s is illustrated in both figures 3.13 and 3.14. Figure 3.13 explain that the conventional used D.T.C attained high dynamic performance in speed response to variations in torque load demand.

At t=0.5s, load disturbance has been introduced. Figures 3.13 and 3.14 show a good dynamic at starting. We also notice from figure 3.14 that the speed regulation loop rejects the applied load disturbance quickly and gain its stability again.

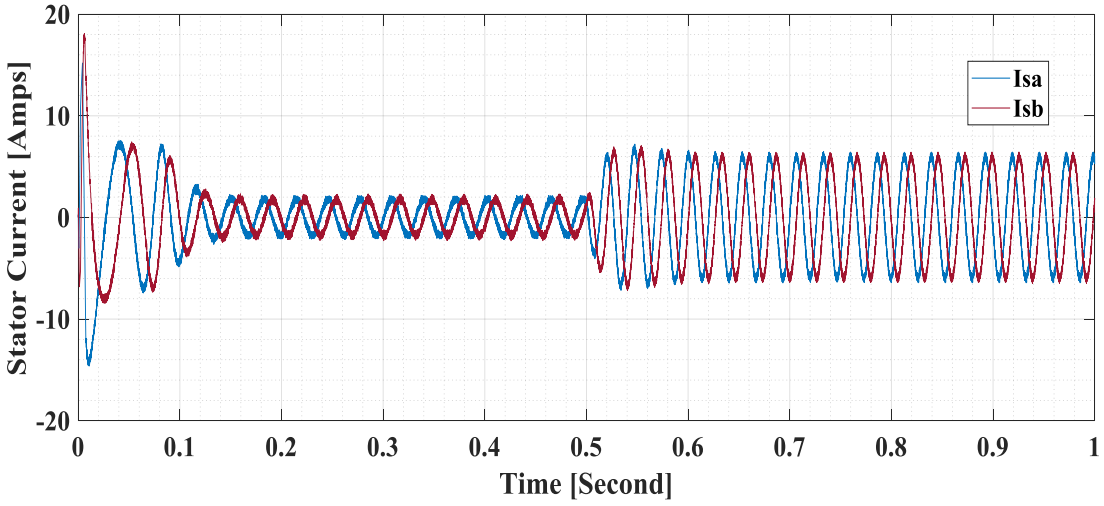

Fig. 3.15- Stator currents

It is noticed from figure 3.15 that the currents' magnitude changes with the change in the load torque. Thus, when a load was introduced at t=0.5s, the currents' magnitude increases in order to satisfies the system requirements.

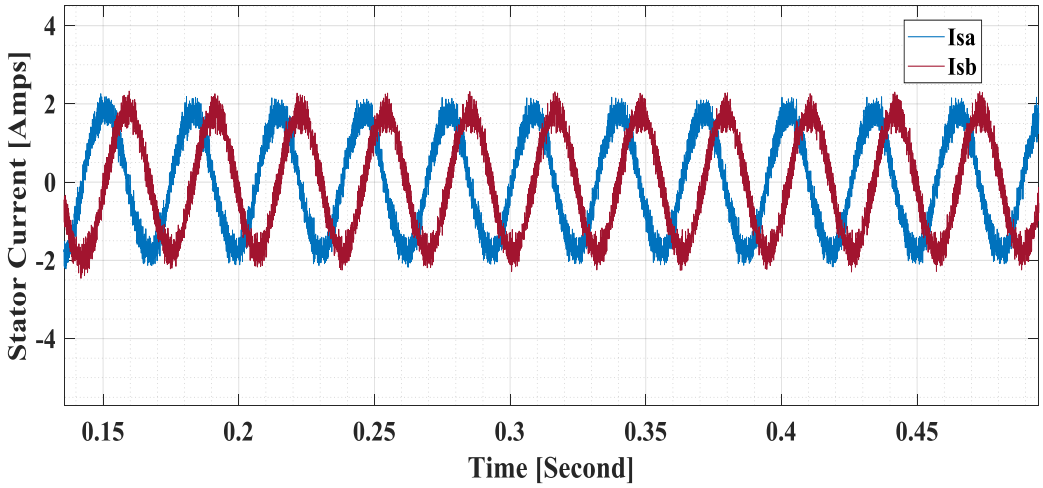

Fig. 3.16- A zoom on Stator currents

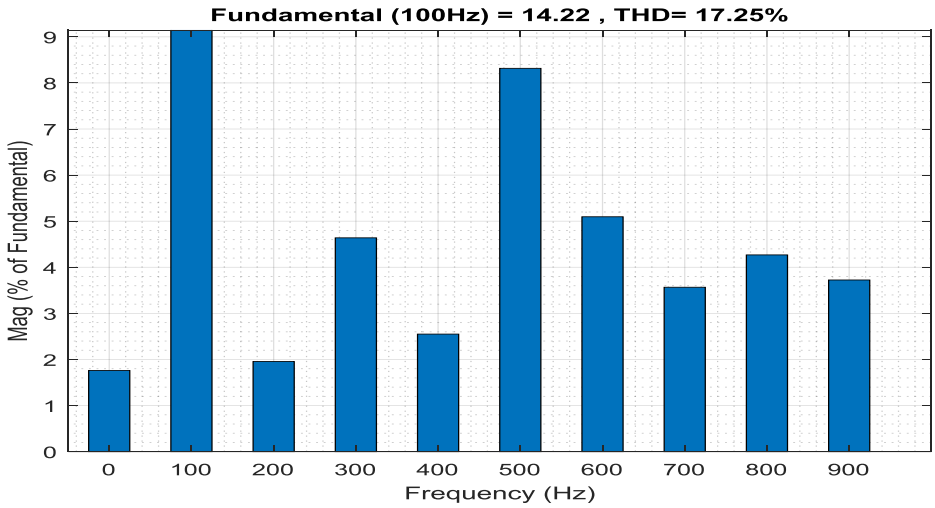

Fig. 3.17- Stator current F.F.T analysis

The stator phase current with zoom and its F.F.T analysis are presented in figure 3.16 and figure 3.17 respectively.

The conventional DTC shows a chopped sinusoid waveform of current which indicates to high harmonics level estimated to 17, 25%.

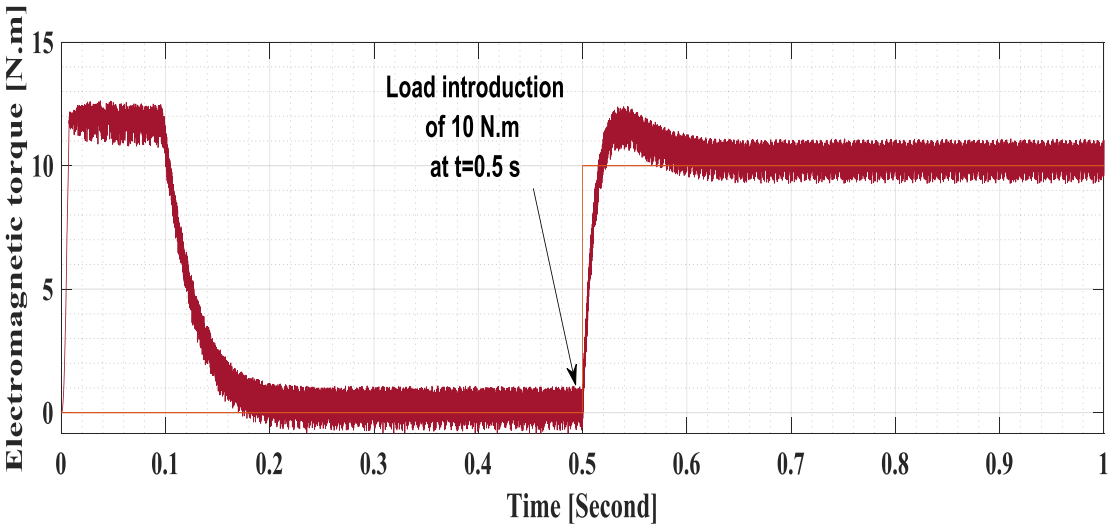

Fig. 3.18- Electromagnetic torque

From figure 3.24 of the electromagnetic torque response , it is seen that at starting the torque has high initial value then decreases sharply to zero because no load is applied .At t=0.5 s the torque increases to 10N.m which is equal to the load torque that is applied at that time and remains same as the load torque raises .

It has been notice that some degradation in performance with overshoot in the torque transient owing to the hysteresis controllers used.

Conclusion:

This chapter displayed the simulation results of the starting up and the steady states without/with load application for the conventional D.T.C controlled an induction motor using MATLAB/Simulink.

The obtained results of both the speed and the electromagnetic torque showed a high dynamic performance to the variation in the load torque as the speed regulation loop rejected the applied load quickly to gain its stability and thus the torque stability also .It has been also noticed that the torque load value change doesn't have control over the flux .

The next chapter will deal with the implementation of this proposed conventional D.T.C in order to compare the simulation results with experimental ones.

4.1.Introduction

This chapter deals with the experimental setup of the implementation of the conventional D.T.C, based on the background introduced in the previous chapters and the simulation done in chapter 03 to consolidate the theoretical analysis of this thesis.

The experimental work was conducted in the Power Research Laboratory at the Institute of Electrical and Electronic Engineering of Boumerdes University. The implementation is conducted for an asynchronous three-phase squirrel cage 1.8kW induction motor using a DSP tms320f28027f.

4.2.Operation description

To assess the control strategy presented in this thesis in real time, an experimental test bench shown in Figure.4.1 is built. The present work consists of a 3-phase power supply supplying a Semikron didactic inverter (see Appendix A.1.2) feeding a 1.8 kW 4 poles squirrel cage induction motor (see Appendix A.1.1). The control algorithm is implemented via a DSP TMS320f28027f Piccolo from Texas Instruments (see Appendix A.1.4.1).The connection between the micro-controller and the power converter is carried out by an interface card (see Appendix A.1.4.2) that adapts the control signal levels called the Dspace from Micro Technologies Lab Company. The main role of this card is to separate between the low power side and the high power side in order to protect the micro-controller. The different current and voltage measurements' are ensured by current and voltage sensor circuits using LA55P and LV25P hall effect sensors respectively. These current circuits are used essentially to measure the actual current for both phases a and b under any operating condition and then are used to compute the (α,β) current components in the stationary (α,β) reference frame. Whereas the hall-effect voltage sensor circuit are used in order to measure the actual dc-link voltage under any operating condition and then to compute the (α,β) voltage in the stationary (α,β) reference frame with the aid of the switching states' (Sa,Sb,Sc) voltage feed-back. In order to monitor the different obtained results a numerical oscilloscope Gwinstek GDS-1042 was used.

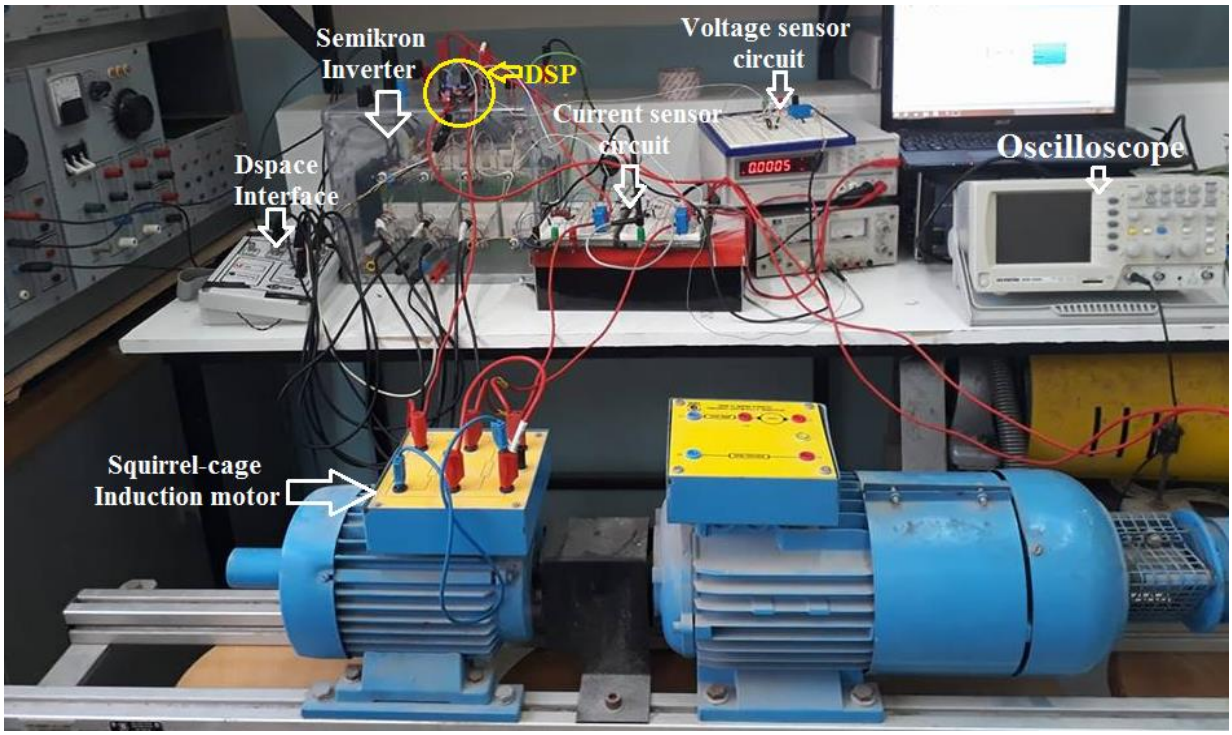

Fig. 4.1 - Implemented test bench of the D.T.C.

4.3.Implementation

4.3.1. Software implementation

The D.T.C algorithm was implemented using DSP TMS320F28027f card. In order to program this card, we have used MATLAB/Simulink C2000 tools.

a. The ADC configuration

In this implementation, four ADCs have been used which are ADCINA0, ADCINA1, ADCINA3 and ADCINA5.

These ADCs were used in order to measure:

- Induction motor Currents (phase a , and phase b);
- U_{dc}voltage;
- The speed from the tachometer.

The A.D.Cs used pins' are shown in Table A.1.4.1.2.

The used DSP ADCs can accept a voltage between [0-3]V, therefore a software compensation must be added in order to remove the incorrectness of the read value. Thus, a calibration of the ADC is a must.

✓ **Calibration of the ADC of DSP TMS320f28027f**

Analog to digital converter with no error in both the gain and the offset follows a linear law expressed as follow:

$$Y = x \times m_i \tag{4.1}$$

Where $m_i$the ideal gain is generally is 1.

$$\text{X= input voltage } * \frac{4095}{3\,V} \tag{4.2}$$

Where x is the input signal.

But in reality there is no ideal gain when using a Hall Effect sensor; so the exact expression of the signal is as follows:

$$Y=x*m_a + b \tag{4.3}$$

Where $m_a$the actual gain, and b is is the actual offset.

Figure.4.2 shows the graph of the input signal using both actual gain and ideal gain.

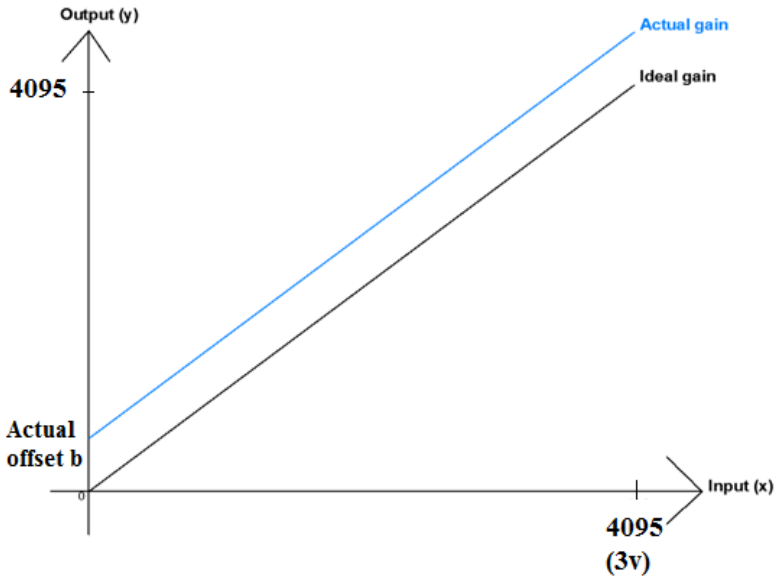

Fig. 4.2 -Graph of the actual and ideal gain.

✓ **ADC output :**

Digital value = 0 …… if Ve≤ $0V$

Digital value = 4095* $\frac{(Ve-ADCL0)}{3}$ ……..if 0V ≤ $Ve \leq 3V$

With ADCL0 is the offset error correction

Digital value =4095 …… if Ve≥3V

✓ **Voltage sensor circuit**

LEM LV 25-P Hall Effect transducer was used in order to sense the voltage. The transducer displays a linear behavior even though an offset is introduced in order to ensure that the output voltage won't exceed 3V.The coefficient of the LV 25-P is 10mA is measured as 25 mA (a=2.5).

Figures 4.3 and 4.4 show the simulated and the implemented voltage sensor circuit.

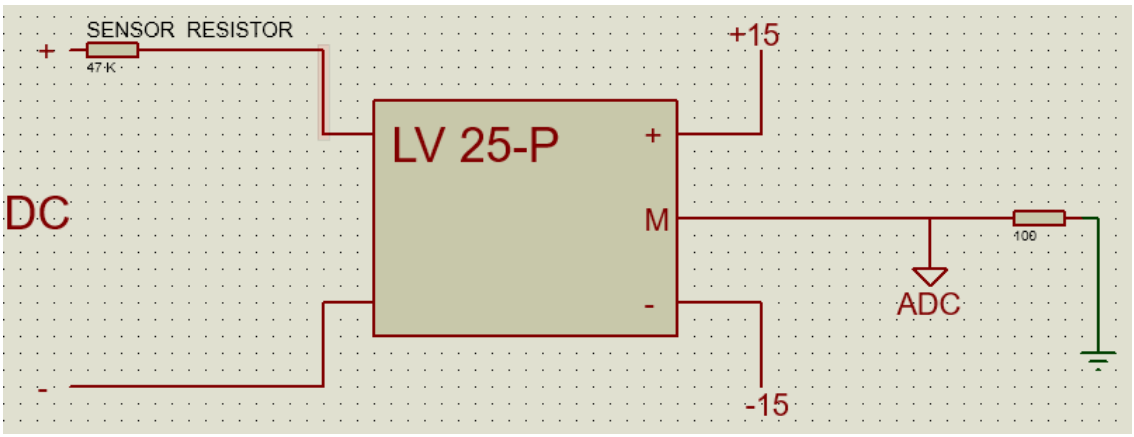

Fig. 4.3 - Circuit of the voltage sensor.

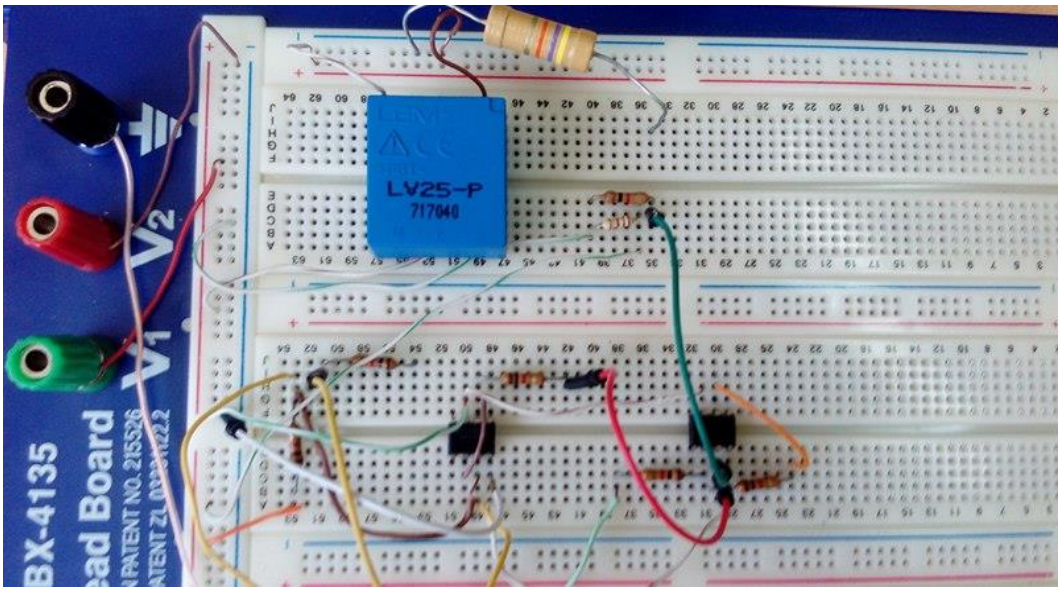

Fig. 4.4 - Implemented circuit of the voltage.

✓ **Current sensor circuit**

LEM LA55-P hall effect transducer was used in order to sense the current. It works with the same principle as the Hall Effect voltage sensor except its ratio of the input current over the output current is (1/1000).

For the case of the motor currents, we have an AC signal thus an offset is introduced in order to shift the current signal and mapped it in the positive quarter. Its circuit is depicted in Figure.4.5.

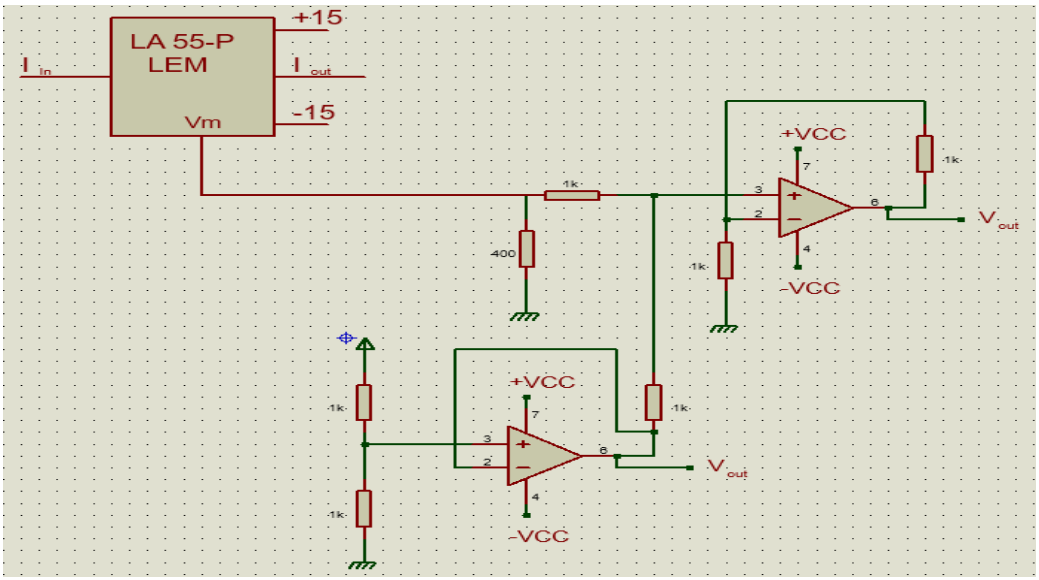

Fig. 4.5 - Current sensor circuit.

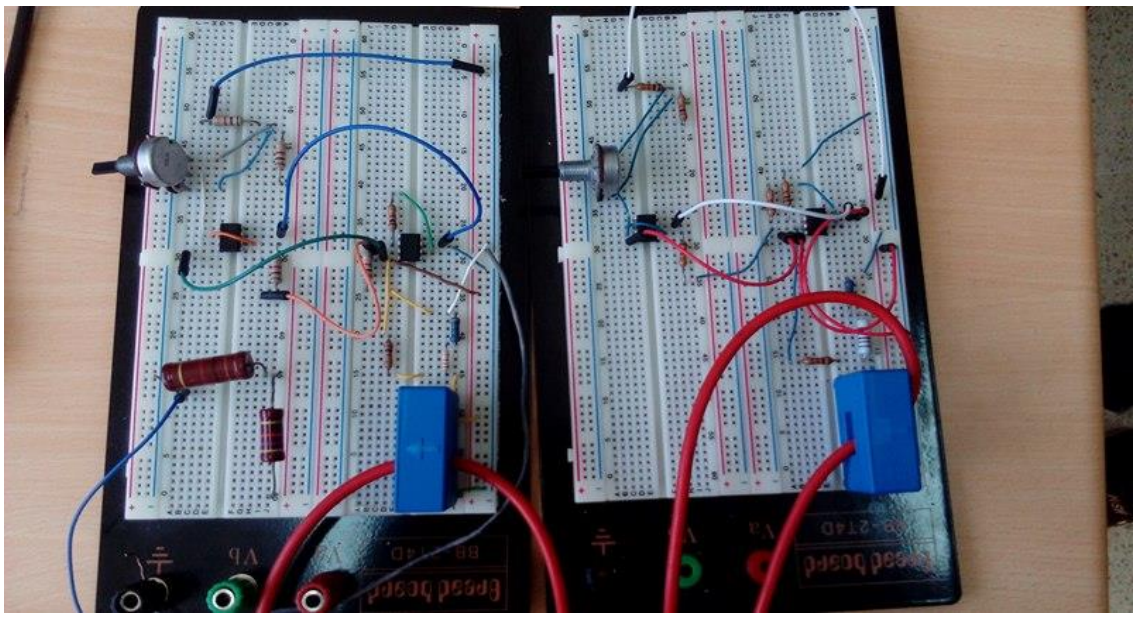

Fig. 4.6 - Implemented current sensor circuit.

From Figure.4.6, we can notice that two hall effect current sensor circuits were built in order to sense two phases of the motor current i_a and i_b. Whereas the third phase i_c is estimated using the software.

b- DSP programming

The algorithm of the DTC was build using Simulink. Figure.4.7 illustrates the Simulink diagram circuit for DTC drive for an induction motor programming for DSP TMS320f28027 using C2000 package.

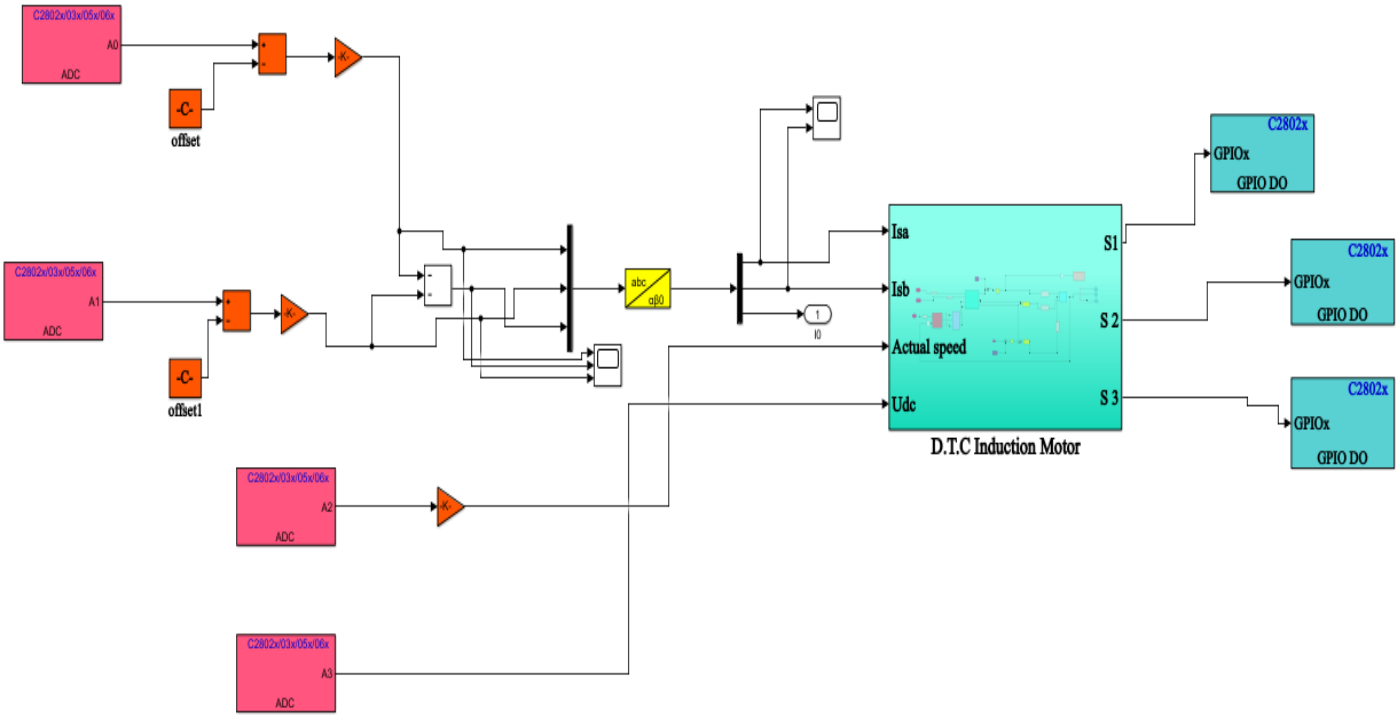

Fig. 4.7 –DSP programming of the DTC for induction motor.

From Figure.4.7 we can see that we have four main parts in the algorithm:

- Voltage estimation ,
- Flux estimation ,
- Switching table command,
- The speed control loop.

➢ **Flux estimator**

Figure 4.8 shows the block diagram of the stator flux magnitude and position.

As the output of the DSP TMS320f28027f is digital, so in order to read the analog signal of the flux a E-pwm with a very high frequency 20kHz is used with a hardware consisting of a low pass filter composed of a resistance of 10kΩ and a capacitor of 1µF as shown in Figure.4.9.

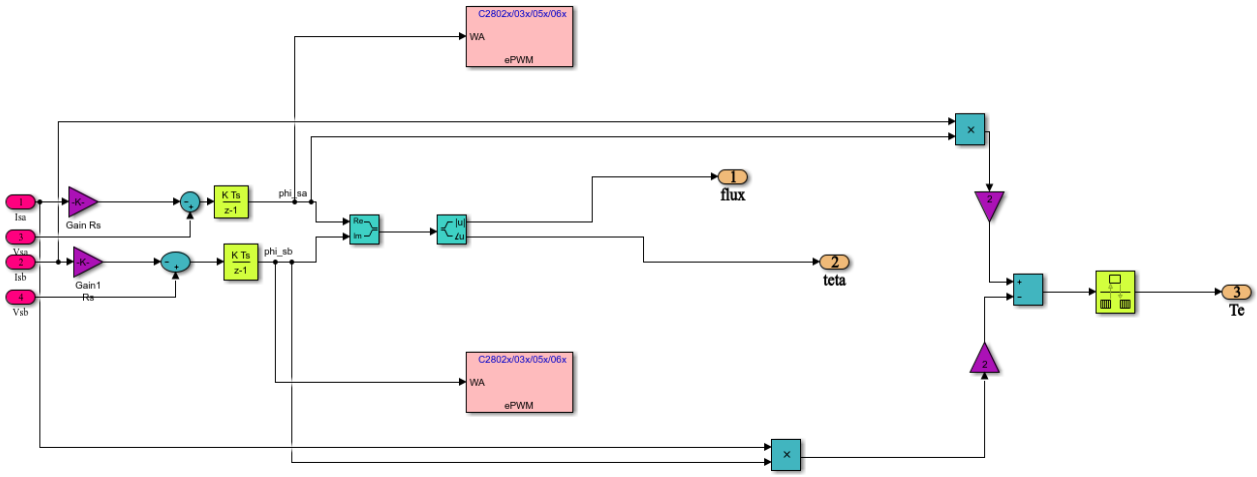

Fig. 4.8 -Flux estimator Simulink block diagram of the DTC for DSP.

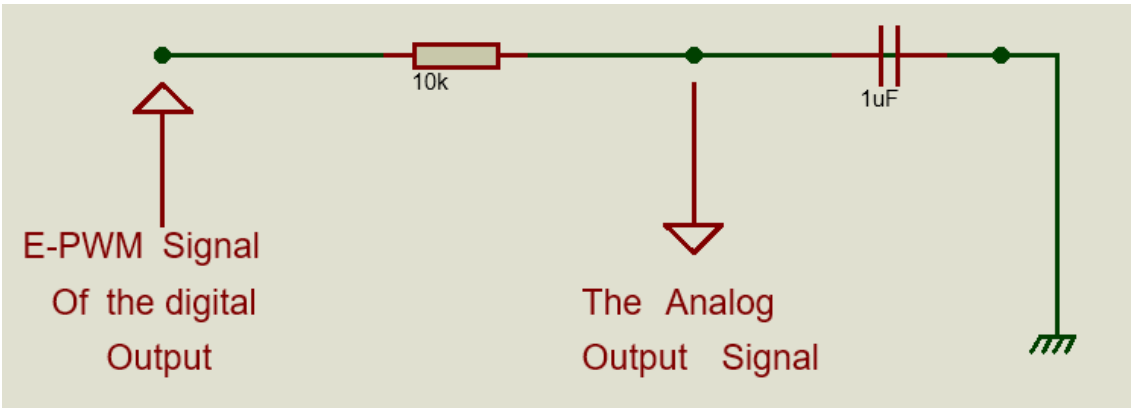

Fig. 4.9 - Low pass filter circuit.

➢ **Switching table**

The switching table command was written as an embedded function. The Matlab code for this table is shown in Appendix A.3.

The stator flux sector determines the appropriate voltage vector from this switching table. This selection generates pulses Sa, Sb and Sc to control the power switches in the inverter and thus generate the 6 possible vectors ($V_1 - V_6$)and two zero vectors ($V_0 - V_7$)as shown in figure 2.2.

- **G.P.I.O estimation**

The GPIO shows the state of the output of the DTC algorithm. The used GPIO pins' were configured according to the pins' location table (Table A.1.4.1.2).
The GPIO represents the switching control signals generated in order to control the switch ON/OFF of the Semikron inverter.

4.3.2. Implementation results compared with the simulated ones:

After implementing the program shown in Figure.4.7, we have obtained the following results which are shown in the Figures 4.10 up to 4.15 as follows:

Figure.4.10 depicts the switching control signals generated by the D.T.C algorithm using DSP TMS320f28027 in order to control the power switches in the Semikron. These signals has the form of PWMs shifted.

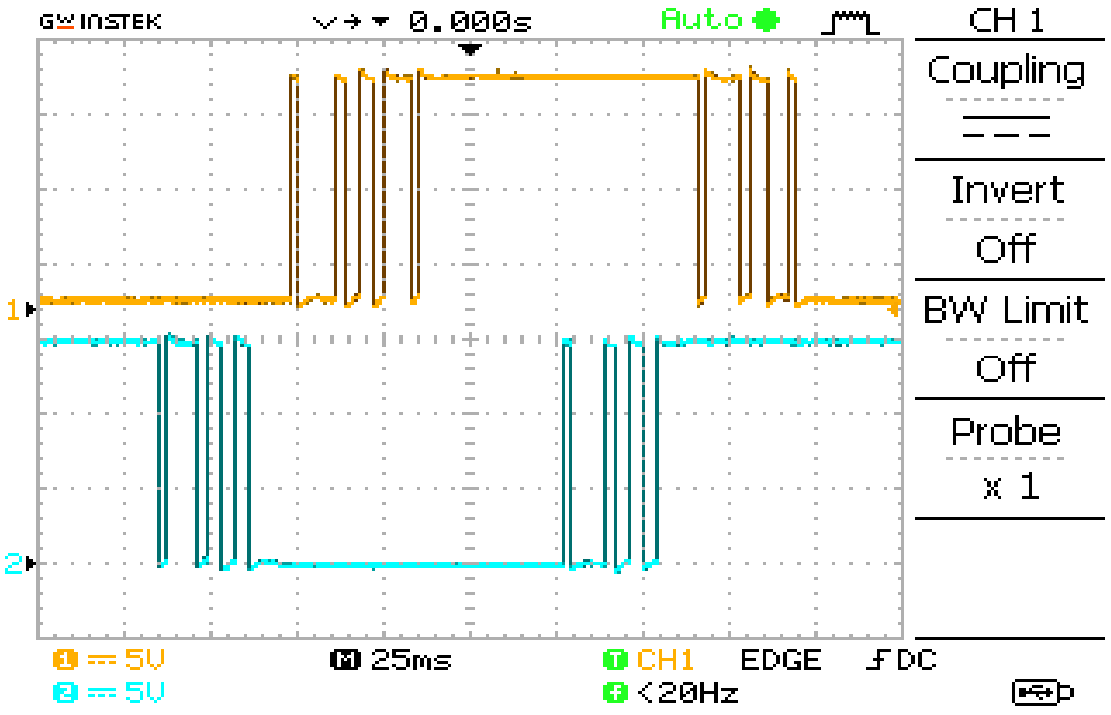

Fig. 4.10- Switching table signals Sa and Sb.

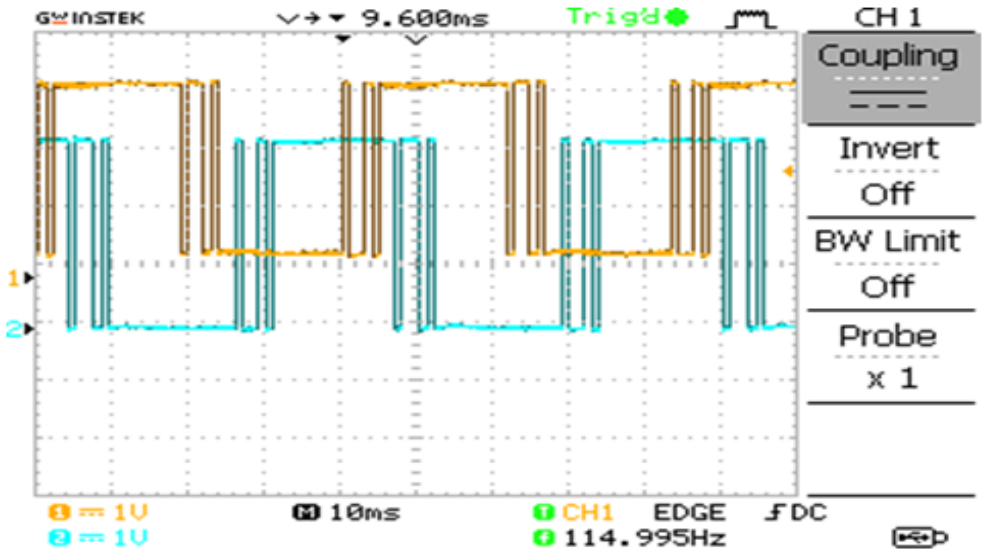

Figure.4.11 presents the stator flux components. These components are in the form of sine-waves. It is noticed that there is a 120° phase shift between the flux on the alpha axis and the one on the beta axis. These curves correspond to the one obtained in the simulation.

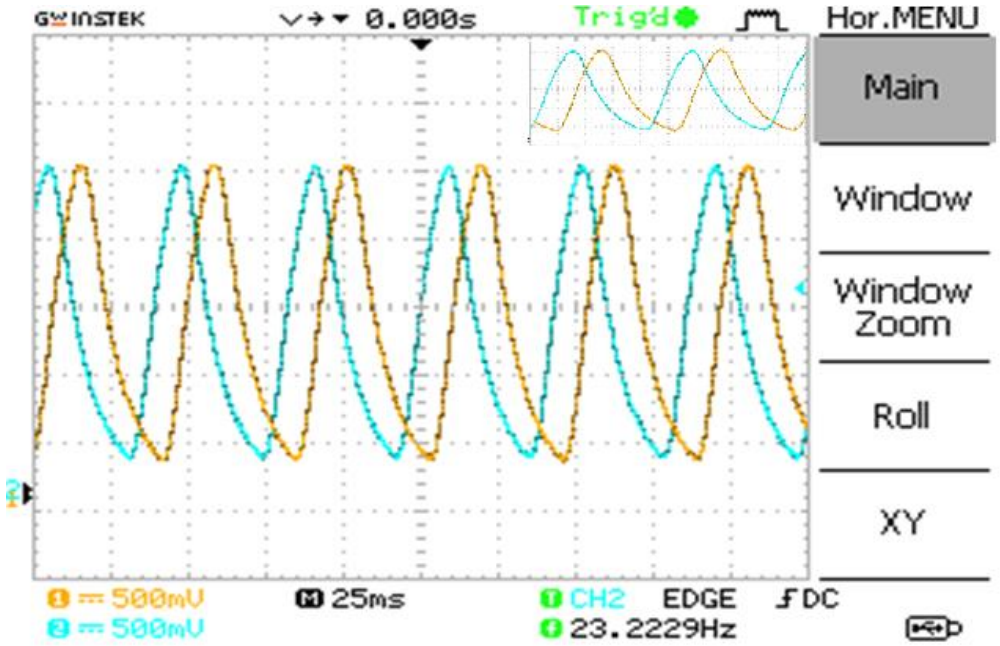

Fig. 4.11 - Stator flux components.

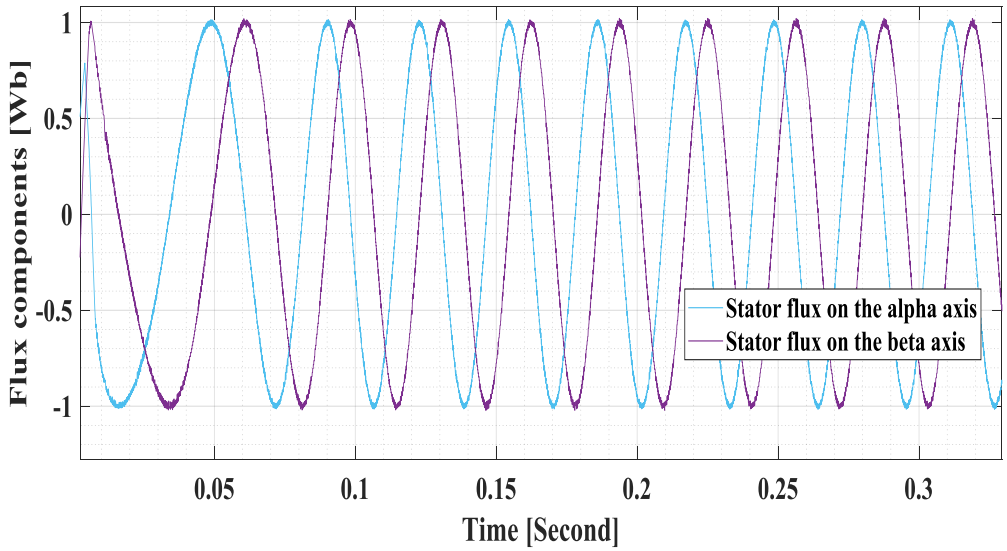

Figure.4.12 represents the stator flux magnitude. This graph corresponds exactly to the one got from the simulation results. We can noticed that the flux varies around a reference value which corresponds to 1Wb.

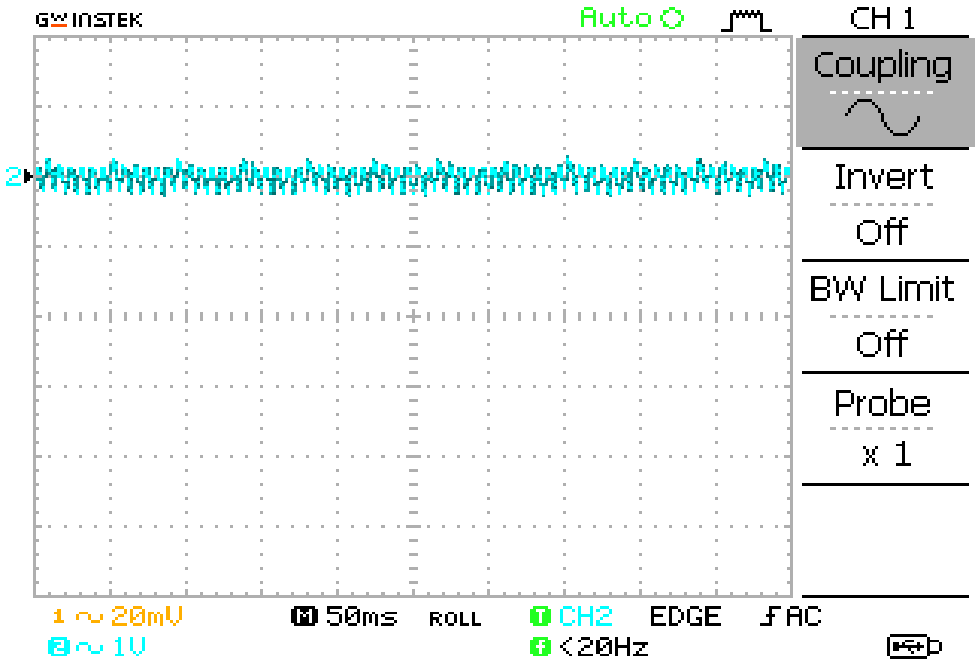

Fig. 4.12 - Stator flux magnitude.

As the flux hysteresis band was reduced to 0.005Wb, the flux locus as seen in figure 4.13 is almost a perfect circle with only very small ripple.

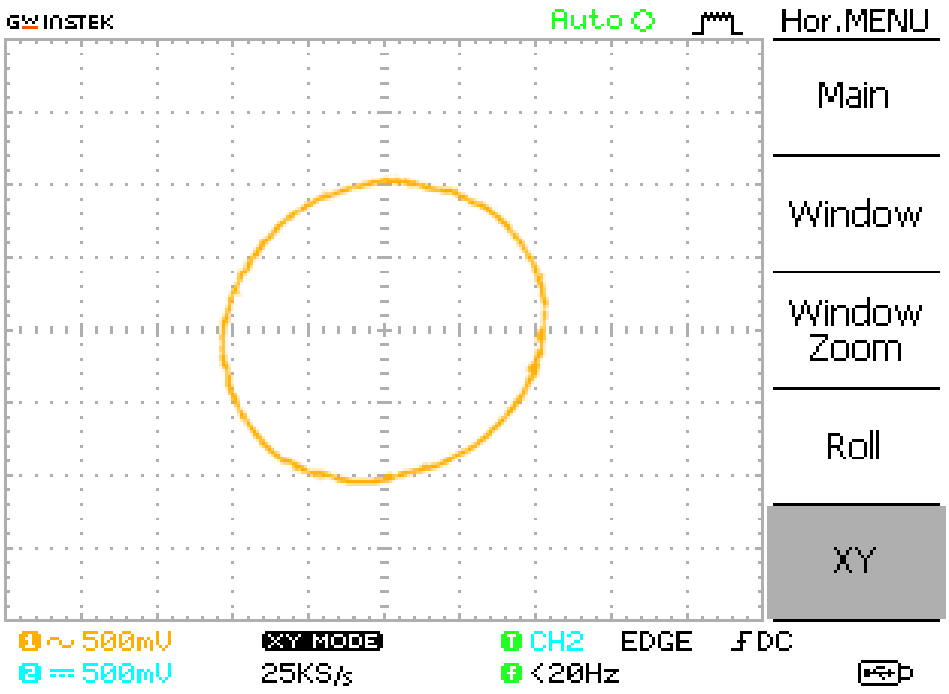

Fig. 4.13 -Flux circular trajectory.

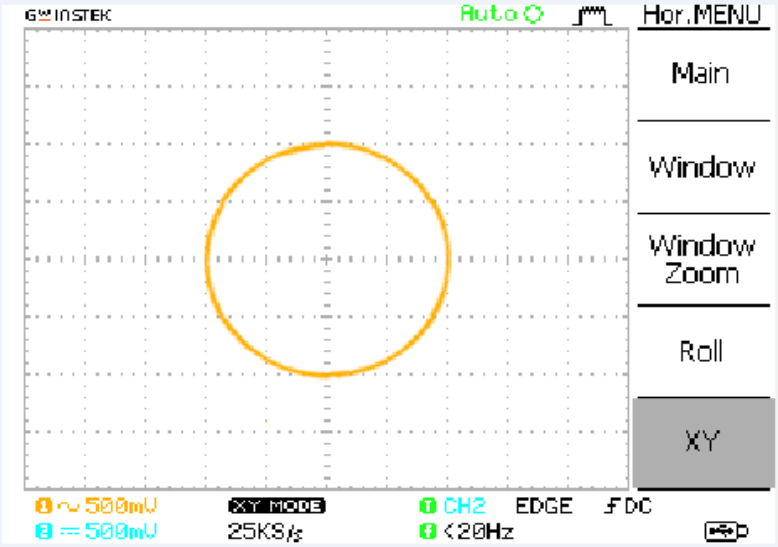

It can be noticed from figure 4.14 that the electromagnetic torque is around 0N.m with only some ripples which corresponds exactly to the theoretical value. As when no load is applied the electromagnetic torque should be 0 N.m.

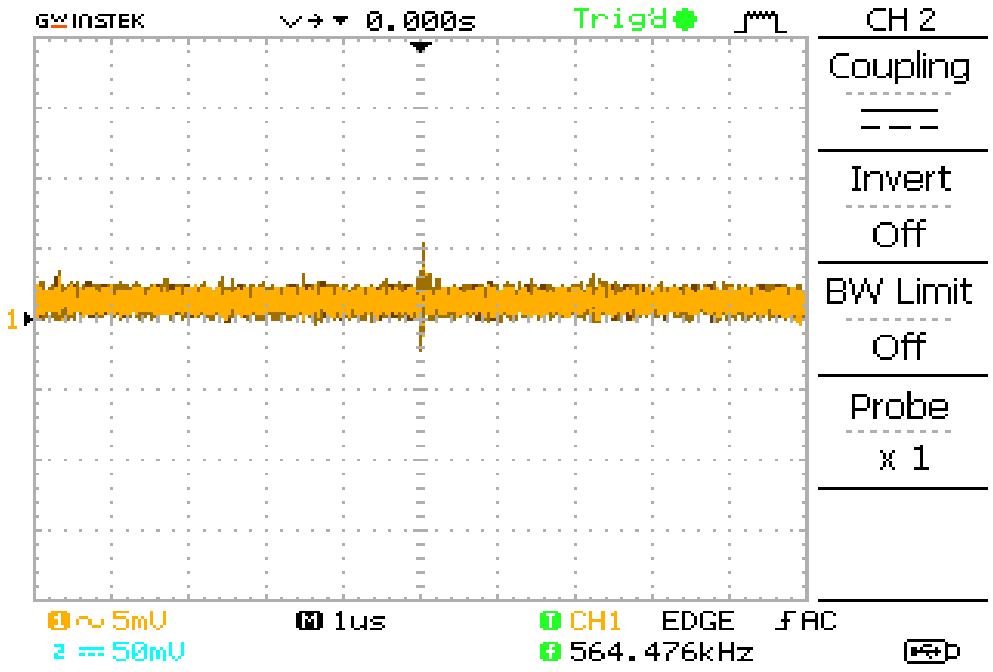

Fig. 4.14 -Electromagnetic torque with no load application.

Figure.4.15 shows the input currents' curves 'i_a' and 'i_b'. As we can see, these curves are almost sine-waves with some distortion due to the harmonics.

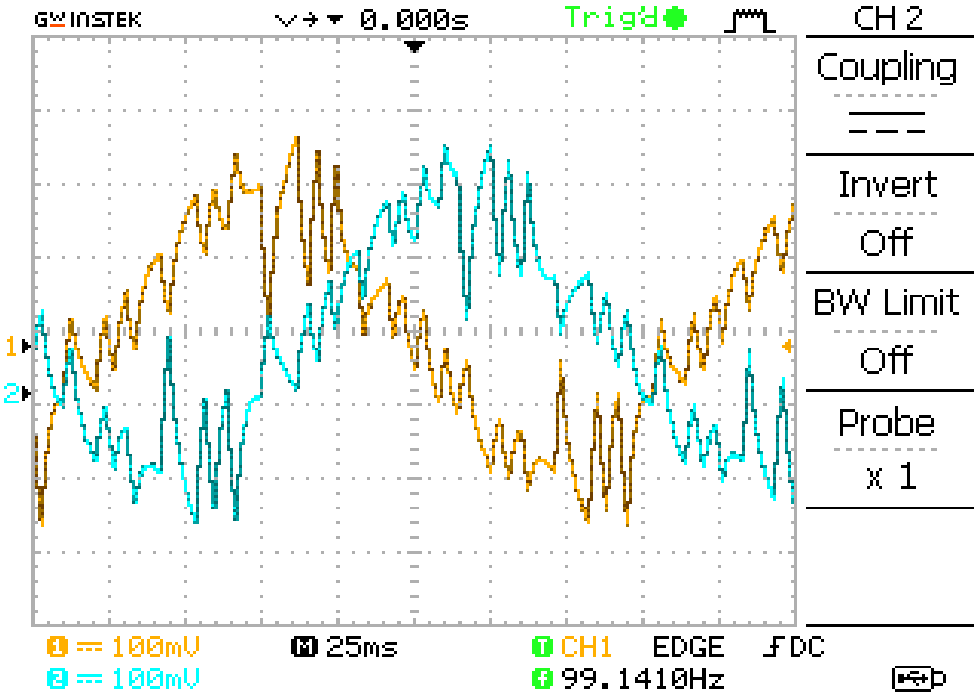

Fig. 4.15 – Input currents i_a and i_b

4.4.Conclusion

This chapter covered the implementation setup and results of the conventional direct torque control drive for an induction motor.

It has been noticed that the implementation and simulation results are approximately the same but with small difference due to some limitations and constraints in the hardware implementation, such as:

- Sensor offset;
- Motor losses as the d-q model is not an exact model for the motor as it doesn't take into consideration the different losses;
- Inverter death time.

From this implementation it can be concluded that this technique is like a sensorless technique as the control of the motor could be achieved even without using the feedback of the speed.

Furthermore, the robustness of this method can be also concluded as the control technique does not depend on the motor's parameters but only on the stator resistance.

General conclusion

5.1. Conclusion

This master thesis validates the proposed model of the conventional direct torque control for an induction motor for an electrical vehicle application. This technique was preferred over the others due to its simplicity, high performance and fast dynamic in motor control.

The designed code was implemented using Matlab/Simulink C2000 package for the C2802x. This programming way is simple and faster comparing to the programming using C.C.S (Code Composer Studio) with C or assembly language. Furthermore, this method is considered cheaper as we can reduce the use of hall effect sensor by help of a feedback from the voltage estimated from the embedded function of the switching table.

Along this dissertation, it has been noticed that the experimental results matched the simulated one which means that the proposed algorithm was effective. During this period, it has been noticed that this type of control method is a sensorless strategy as it can work even without speed feedback. Also, it is a low cost strategy drive which require less number of ADCs, in order to measure the phase currents, the DC voltage and speed meaning three Hall Effect sensors but it is not mandatory as it can work only with the DC voltage measurement of Course with the help of the feedback voltage from the switching table.

5.2. Future work

Even though, the direct torque control is considered as a robust and low-cost driving strategy for an induction motor but it has also some drawbacks. These latter are expressed by:

- The high harmonics and ripples in the currents and torque.
- The algorithm is dependent only on the stator resistance. Thus, any variation in this later will introduce error in the stator flux linkage computation.

Therefore, some adaptation and amelioration are planned for next work in order to overcome the limitation of the used conventional DTC which are:

- The use of 12 twelve sectors to control the switching of the three-level inverter to achieve reduced harmonics distortion.
- The use of a sensorless algorithm in order to increase the reliability of the system.
- The use of S.V.M with fixed switching frequency to reduce switching losses.

A.1 Appendix 1 : Material used for the simulation Real Time Implementation of the direct torque control for the induction motor .

A.1.1.Induction motor parameters

In this dissertation both in the simulation and the implementation, a three-phase squirrel cage induction motor has been used.

Its parameter are shown in table.A.1.1.

Table A.1.1- Parameters of the induction motor.

Machine's Power	1.8 kW
Current	3.8A / 5A
Voltage	380V/400V
Stator resistance	5.06 ohm
Maximum speed	1446 rpm

A.1.2.Semikron Inverter

SEMIKRON Inverter is a three-phase IGBT rectifier with two level inverter with brake chopper (V_{AC}=400,I_C =30A).Its picture is depicted in figure A.1.2.

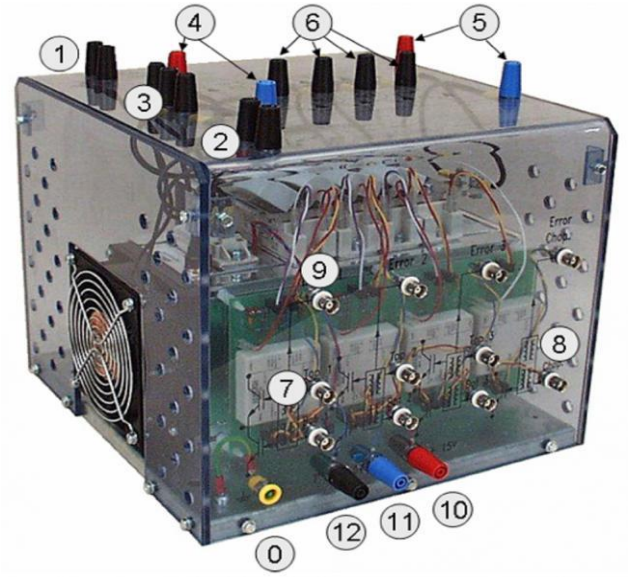

Fig. A.1.2- Semikron Inverter.

From figure A.1.2, it can be noticed that the Semikron Inverter is composed of :

- **No.1 :** Cooling system
- **No.2 :** Interruption relay in series with the alimentation of 15 V.
- **No.3 :** Inverter inputs
- **No.4 and 5 :** Input/Output of the DC bus (terminals of the filter capacitor)
- **No.6:**Inverter terminals
- **No.7:**Inverter sears
- **No.8:** Boost sears
- **No.9:**error signals
- **No.10 and 11:** Alimentation drivers
- **No.12:** Temperature relay

The characteristics of the used Semikron Inverter Table are shown in table A.1.2.

Table A.1.2- Semikron Inverter characteristics.

Symbol	Conditions	Values	Units
I_{rms}	no overload	30	A
	IGBT - 4x SKM 50 GB 123D		
V_{CES}		1200	V
$V_{CE(SAT)}$	I_c= 50A, V_{GE}= 15V, chip level; T_j= 25(125)°C	2,7 (3,5)	V
V_{GES}		±20	V
I_C	T_{case}= 25 (80)°C	50 (40)	A
I_{CM}	T_{case}= 25 (80)°C; t_p= 1ms	100 (80)	A
	Rectifier - 1x SKD 51/14		
$V_{in(max)}$	without filter	3 x 480	V
	with filter	3 x 380	V
	DC Capacitor bank - Electrolytic 2x 2200µF/400V		
C_{eqvl}	total equivalent capacitance	1100 / 800	µF / V
V_{DCmax}	max. DC voltage applied to the capacitor bank	750	V
	Driver - 4x SKHI 22		
Power supply		0 / 15	V
Current consumption	max; per driver	16	mA
Thermal trip	Normally Open type (NO)	71	°C

A.1.3.Lead Acid batteries:

Valve Regulated Lead Acid (VRLA) batteries are the most widely used type because of their high power density and ease ofuse. These batteries come in all shapes, voltages, amperages and sizes. VRLA batteries are considered tobe “sealed” because they normally do not allow for the addition or loss of liquid. The term VRLA derives from the use of safety valves that allow pressure to be released when a fault condition causes internalgas to build up faster than it can be recombined.

They are three types of VRLA:

1. Sealed valve regulated wet cell.
2. Absorbed Glass Mat (AGM).
3. Gel.

VRLA batteries offer a lot of advantages over other types of batteries, such as:

- Maintenance Free
- Moderate life
- High right capacity
- High charge efficiency
- State of charge can be determined by measuring the voltage
- Available in a variety of size and voltages

Fig. A.1.3-YUASA battery.

The characteristics of the available Valve Regulated Lead Acid battery NP38-12 I of YUASA depicted in figure A.1.3 is shown in table A.1.3.

Table A.1.3-YUASA battery characteristics.

Maximum rated voltage	13.50-13.70 V
Maximum Capacity	40 Ah
Rated Capacity	38 Ah

A.1.4.Digital control implementation

A.1.4.1.DSP TMS320f28027f :

DSP Piccolo TMS320f28027fpresented in figure A.1 is texas instruments' microcontroller that provides the power the C28x core coupled with highly integrated control peripherals in low pin-count devices. This family is code-compatible with the previous C28-based code,and also provides a high level of analog integration .The table below 4.1 shows some of the technical characteristics needed to be known in this implementation .

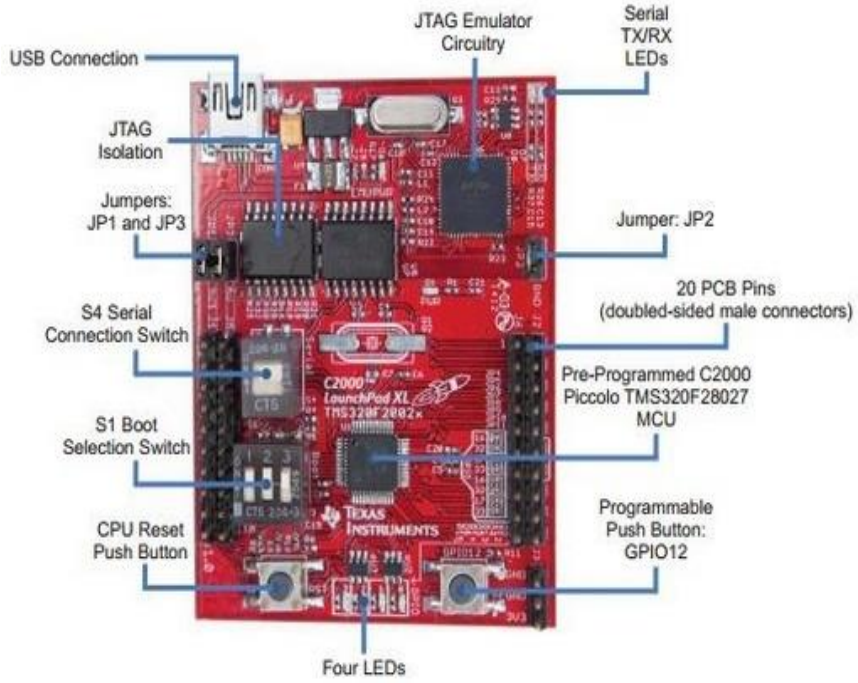

Fig. A.1.4.1-DSP TMS320f28027f

Table A.1.4.1.1- Some of the technical characteristics of DSP

C.P.U	C28x
Total processing	60 MIPS
Frequency	60Mhz
Flash	64 KB
R.A.M	12 KB
A.D.C resolution	12-bit
A.D.C channels	13(7A-6B)
E-PWMs	8
GPIO (can be configured as input or as output)	22/22

Table A.1.4.1.2-Pins' location on the DSP

Mux Value						Mux Value			
3	2	1	0	J1 Pin	J5 Pin	0	1	2	3
			+3.3V	1	1	+5V			
			ADCINA6	2	2	GND			
TZ2	SDAA	SCIRXDA	GPIO28	3	3	ADCINA7			
TZ3	SCLA	SCITXDA	GPIO29	4	4	ADCINA3			
Rsvd	Rsvd	COMP2OUT	GPIO34	5	5	ADCINA1			
			ADCINA4	6	6	ADCINA0			
	SCITXDA	SPICLK	GPIO18	7	7	ADCINB1			
			ADCINA2	8	8	ADCINB3			
			ADCINB2	9	9	ADCINB7			
			ADCINB4	10	10	NC			
3	2	1	0	J6 Pin	J2 Pin	0	1	2	3
Rsvd	Rsvd	EPWM1A	GPIO0	1	1	GND			
COMP1OUT	Rsvd	EPWM1B	GPIO1	2	2	GPIO19	SPISTEA	SCIRXDA	ECAP1
Rsvd	Rsvd	EPWM2A	GPIO2	3	3	GPIO12	TZ1	SCITXDA	Rsvd
COMP2OUT	Rsvd	EPWM2B	GPIO3	4	4	NC			
Rsvd	Rsvd	EPWM3A	GPIO4	5	5	RESET#			
ECAP1	Rsvd	EPWM3B	GPIO5	6	6	GPIO16/32	SPISIMOA/ SDAA	Rsvd/ EPWMSYNCI	TZ2/ ADCSOCA
TZ2/ ADCSOCA	Rsvd/ EPWMSYNCI	SPISIMOA/ SDAA	GPIO16/32	7	7	GPIO17/33	SPISOMIA/ SCLA	Rsvd/ EPWMSYNCO	TZ3/ ADCSOCB
TZ3/ ADCSOCB	Rsvd/ EPWMSYNCO	SPISOMIA/ SCLA	GPIO17/33	8	8	GPIO6	EPWM4A	EPWMSYNCI	EPWMSYNCO
			NC	9	9	GPIO7	EPWM4B	SCIRXDA	Rsvd
			NC	10	10	ADCINB6			

From the table A.4.2.1.2, it can be seen the used pins' location in order to connect correctly the hardware to the DSP card and also read the exact output .

This card can be programmed whether using Code Composer Studio in C,C++ or assembly language or using Matlab/Simulink C2000 support package.

A.1.4.2.2.Dspace interface board

Dspace interface it is Micro-technologies Lab equipments .It is dedicated to universities or research and development companies. It is an adaptation and isolation interface which separates between the high power side and the low power side in order to protect the micro-controllers. Its picture is depicted in fig. A.1.4.2.

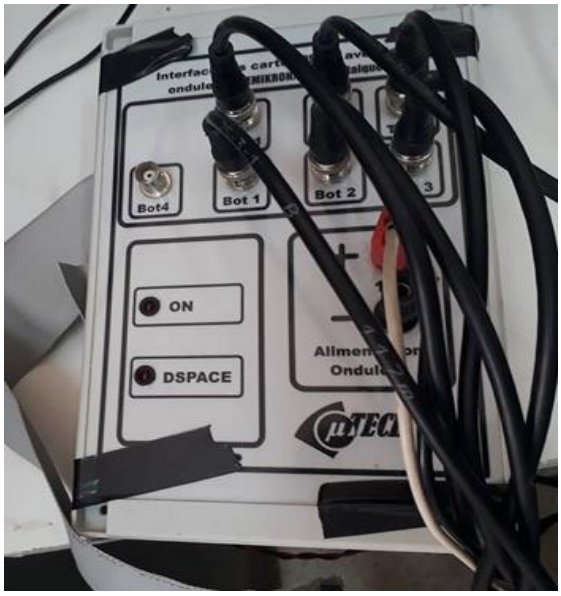

Fig. 1.4.2.2-Dspace interface board

A.2 Appendix 2 : Speed PI controller's gain calculation

For the speed loop for the DTC an anti windup controller PI is used.
The dynamic equation and the transfer function using Laplace transform of the speed loop are given as following :

$$\frac{dw_r}{dt} = -\frac{f}{J}w_r + \frac{T_e}{J} - \frac{1}{J}T_L$$

$$G_{wr}(s) = \frac{w_r(s)}{T_e(s) - T_L(s)} = \frac{1}{Js + f}$$

The transfer function of the PI controller is defined as follow :

$$\text{PI}=K_p s+\frac{K_i}{s}$$

Where :K_p and K_i are the proportional and integrator gains ;

And S is the Laplace operator.

Then , figure A.2.1 shows the block diagram of the speed control loop

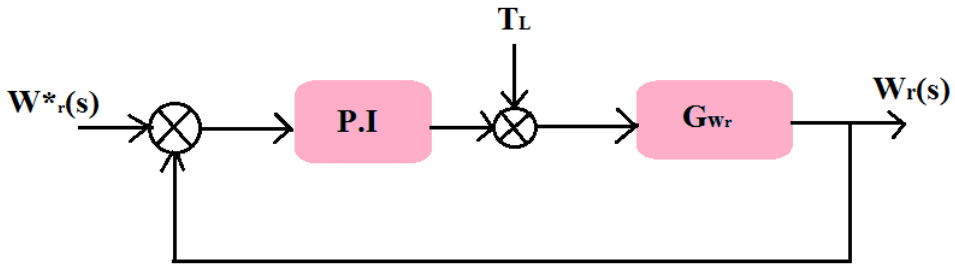

Fig. A.2.1- Speed control loop block diagram

By considering the load torque T_L as a disturbance .The global transfer function of the speed control in open loop becomes

$$G_{wr}(s) = \frac{w_r(s)}{w_r^*(s)} = \frac{1}{Js+f}(K_p s + \frac{K_i}{s})$$

In closed loop , the TF becomes

$$G_{wr}(s) = \frac{(K_p s + K_i)}{Js^2 + (K_p + f)s + K_i}$$

By identification member to member , the denominator of the equation … with the canonical form of second order system given in ….:

$$G(s) = \frac{1}{s^2 + 2\xi w_n s + {w_n}^2}$$

Where w_n is the natural frequency and $\xi$is the damping coefficient

We obtain :

$$\begin{cases} \frac{J}{K_i} = \frac{1}{{w_n}^2} \\ \frac{K_p + f}{J} = 2\xi w_n \end{cases}$$

The gains are determined for a damping coefficient $\xi = 1$.

References

[01]Austin Hughes "Electric Motors and Drives Fundamentals,Types and applications".Thirdedition.Elsevier Ltd.2006.

[02]Husain,Iqbal "Electric And Hybrid Vehicles: Design Fundamentals".Third edition. pp1,2005.

[03]Jaroslav Lepka,Petr Stekl "3-phase AC Induction Motor Vector Control Using 56F80x,56F8100 or 59F8300Device.Freescale Semiconductor Application Note",2005.

[04] Merlin Gerlin,Cahier technique no.204,Electric motors and how to improve their control and protection.E.Gaucheron.Schneider Electric.

[05] Neha, Sharma, Vijay Kumar, Garg "A comparative Analysis of Scalar and Vector Control of Induction Motor Drive".

[06]BehzaAsaei,MohammadNaser Hashemnia.Comparative Study using Different Electric Motors in the Electric Vehicles. ICEM,18th International conference, 2008.

[07]U. Baader, M. Depenbrock and G. Gierse "Direct Self Control (DSC) of Inverter Fed-Induction Machine, A basis for speed control without speed measurement". IEEE Trans. Ind. Application. 28:pp 581- 588, 1992.

[08]M. Depenbrock "Direct self-control of the flux and rotary moment of a rotary-field machine. U.S. Patent" 4 678 248. July 7, 1987.

[09]R Kennel,EE El-Kholy,S Mahmoud,A El-refaei,F Elkady."Improved direct torque control for induction motor drives with rapid prototyping system".Energy conversion and management.2006.

[10] El-Zefery "High Performance Direct Torque Control for Induction Motor Drive Fed From Photovoltaic System".Word Academy of Science,Engineering and Technology International Journal of Energy and Power engineering.Vol9, No 11,.2015.

[11]I. Takahashi and T. Noguchi "A New Quick Response And High Efficiency Control Strategy Of An Induction Machine". IEEE Trans. Ind. Applica.22:pp 820 827,1986.

[12]U.Shajith Ali,V.Kamaraj "A Modified Space Vector PWM For Bi-Directional Z-SourceInverter".ICETECT, 2011.

[13]Abdelkarim Ammar "Improvement of Direct Torque Control Performances for Asynchronous Machine using Non-Lineartechniques".Ph.Dthesis.University of Biskra, 2017.

[14] Vudatha Vinod Kumar "Analysis Of Induction Motor Drive With Direct Torque Controlscheme Using Space Vector Modulation".Masterthesis.National Institute of Technology,Orissa,India.2015.

[15] Cristian, Lascu, Boldea, Blaabjerg "A Modified Direct Torque Control for InductionMotor Sensorless Drive" IEEE transaction on Industry Applications, Vol.36, No.1, Jan/Feb 2000.

[16]www.grandviewresearch.com/press-release/global-electric-ac-motors-market[2012].